CORROSION OF ALUMINUM ALLOY 2024 BELONGING TO THE 1930s IN SEAWATER ENVIRONMENT

A Thesis

by

KEDAR GUJARATHI

Submitted to the Office of Graduate Studies of
Texas A&M University
in partial fulfillment of the requirements for the degree of

MASTER OF SCIENCE

August 2008

Major Subject: Mechanical Engineering

CORROSION OF ALUMINUM ALLOY 2024 BELONGING TO THE 1930s IN SEAWATER ENVIRONMENT

A Thesis

by

KEDAR GUJARATHI

Submitted to the Office of Graduate Studies of
Texas A&M University
in partial fulfillment of the requirements for the degree of

MASTER OF SCIENCE

Approved by:

Chair of Committee,	Richard Griffin
Committee Members,	Hong Liang
	Thomas Pollock
Head of Department,	Dennis L. O'Neal

August 2008

Major Subject: Mechanical Engineering

ABSTRACT

Corrosion of Aluminum Alloy 2024 Belonging to the 1930s in Seawater Environment.

(August 2008)

Kedar Gujarathi, B.En. University of Pune, India

Chair of Advisory Committee: Dr. Richard Griffin

Wreckage of '*Carnauba*', a 1930s vintage Sikorsky S-38 aircraft, a beloved icon of SC Johnson's early history, was found on July 5, 2000, in seawater off of an Indonesian island of West Irian Jaya. The company decided to recover this aircraft from seawater, conserve it, and display it in its museum, as part of their rich heritage. The objective was to study the aluminum alloy used on the aircraft for its chemical and mechanical properties, suggest the corrosion mechanism of aluminum alloy 2024 in seawater, and recommend preservation methods for the same. Chemical analysis performed on the samples collected from the site revealed that copper was the primary alloying element. Copper is responsible for increasing the strength. However, copper is also the reason for pitting corrosion of the aluminum alloy, causing material loss and reducing the structural stability of the wreckage. Copper forms intermetallics with other elements, such as magnesium and aluminum, and is distributed in the aluminum matrix heterogeneously. In order to study the corrosion mechanism of aluminum alloy 2024, it was subjected to potentiodynamic tests in sodium chloride solution. In the presence of an

electrolyte like seawater, the difference between the potentials of these intermetallics and the surrounding aluminum matrix creates a galvanic cell. The galvanic cells serve as sites for localized corrosion. Chloride ions are responsible for pitting of alloy 2024. A pitting potential of around -600mV was observed when sodium chloride was used as an electrolyte. The average corrosion rate measured for wrought aluminum alloys was around 0.05 mm/year. The thesis provides guidelines or recommendations for the procedure to be followed in recovering aircraft from seawater, and retain it in its as found condition. Recommendations about various measurements like pH, dissolved oxygen, salinity, pressure, temperature, and velocity need to be taken and the visual assessment needs to be done before the aircraft is hauled from the seawater were specified. After the aircraft has been recovered, recommendations for handling, cleaning, and prevention of corrosion using coatings such as carnauba wax and inhibitors such as chromates, have been stated.

ACKNOWLEDGMENTS

I would like to thank my research advisor, Dr. Richard Griffin, for his patience, guidance and support over the course of this research. He was a constant inspiration, and his assistance and suggestions were invaluable towards the completion of this work. I would also like to thank the members of my exam committee, Dr. Hong Liang and Dr Thomas Pollock, for their efforts in reviewing and evaluating my research. I would like to acknowledge and thank the Department of Mechanical Engineering at Texas A&M University for the various opportunities that have helped to make this journey an educational as well as an enjoyable one. I would also like to thank Dr. Esam Husain for his helpful insights and invaluable suggestions.

I would like to dedicate this research work to my family. To my parents, who have always encouraged me to pursue my goals, always succeed, and never admit defeat. From them I have learned to be the best that I can be. Thank you for being a part of my life.

TABLE OF CONTENTS

Page

Page

LIST OF FIGURES

Page

Page

Page

LIST OF TABLES

Page

1. INTRODUCTION

We often come across artifacts in technical museums made of pure metals and their alloys [1]. The Lockheed P-38 Lightning fighter aircraft, presumed to be USAAF serial number 41-7677, emerged from the sand of a beach in Wales where it crash landed in 1942. Two intact Douglas "Devastator" torpedo bombers have been found in relatively shallow water on the bottom of Jaluit lagoon in the Marhsall Islands. These aircraft not only represent the best surviving examples of their type but they are also individually historic [Courtesy of The International Group for Historic Aircraft Recovery, TIGHAR, Wilmington, Delaware]. Many of these artifacts have been recovered from seawater, and date back several decades. Although these artifacts are relatively recent in archaeological terms, one often wonders how these artifacts survived the degradation due to seawater over the course of time. These metallic artifacts are of particular interest to us, as their modifications and in most cases, improved versions are still manufactured today. Such objects include a number of aeronautical artifacts recovered from rivers and oceans, most of them belonging to the era of the last two world wars. People attribute sentimental and technological value to these artifacts, and as such their recovery and study is a cultural, as well as an archeological pursuit. The examination and analysis of the artifacts gives us an idea about the type and the quality of fabrication processes available during the era the artifact belongs to. One can also compare the artifact materials and designs to the contemporary ones.

This thesis follows the style of *Studies in Conservation*.

Samuel C. Johnson was the chairman emeritus of SC Johnson Wax and was as devoted to aviation as his father, who in 1935 flew a Sikorsky S-38 amphibian plane to Brazil in search of *Carnauba* palms, a key ingredient in wax. The wonderful amphibian biplane that had carried Samuel Curtis Johnson's father all the way to Brazil in 1935 had unceremoniously sunk to the bottom of Manokwari Bay, Indonesia, in 1938. The location of the wreckage site is shown in Figure 1.1. *Carnauba* airplane (S-38), a 1930s vintage aircraft is a beloved icon of SC Johnson's early history. It was found off the shores of Manokwari Bay, in 90 feet of water in a debris field.

On June 27, 2000, SC Johnson Chairman and CEO Fisk Johnson, son of S.C. Johnson and his family embarked on an expedition to search for the wreckage of the Sikorsky S-38 plane. They successfully found the wreckage on July 5, 2000, and planned to retrieve its remains and conserve the aircraft in their family museum. For the Johnson family, great sentiment and history are associated with this aircraft. This study is part of the retrieval plan. One of the objectives of the study is to recommend steps to be taken to conserve the aircraft. One needs to study the aluminum alloy used to manufacture the Sikorsky S-38 and propose a corrosion mechanism for the aluminum alloy. One would also be curious to know the advances in the development of aluminum alloys since 1930s and their typical application in the aerospace industry.

Figure 1.1 Location of the Carnauba wreckage site.

When one finds a wreckage site, there is a desire to recover and study it. However, a number of unfortunate recent experiences (the Arado 96 [2] and the Dornier 24s [3] from the lakes of Landes) have demonstrated the unstable nature of these types of objects when exposed to the atmosphere. The corrosion already present rapidly exacerbates, significantly diminishing the time required for complete metal destruction. Studies on aircraft wreckages around the world have been undertaken during the past. Figure 1.2 shows a Junkers W33 aircraft which was abandoned by H. Bertram, at Cape Bernier (14°00'S, 127°27'E) in 1932[4] is an example. Treatment of BMW Aero Engine from the Loiret River in 1992[5], is another. There is a huge scope for studying the corrosion behaviour of components found in the huge repositories of wrecks available around the world and eventually, develop a technique to preserve these historical artifacts.

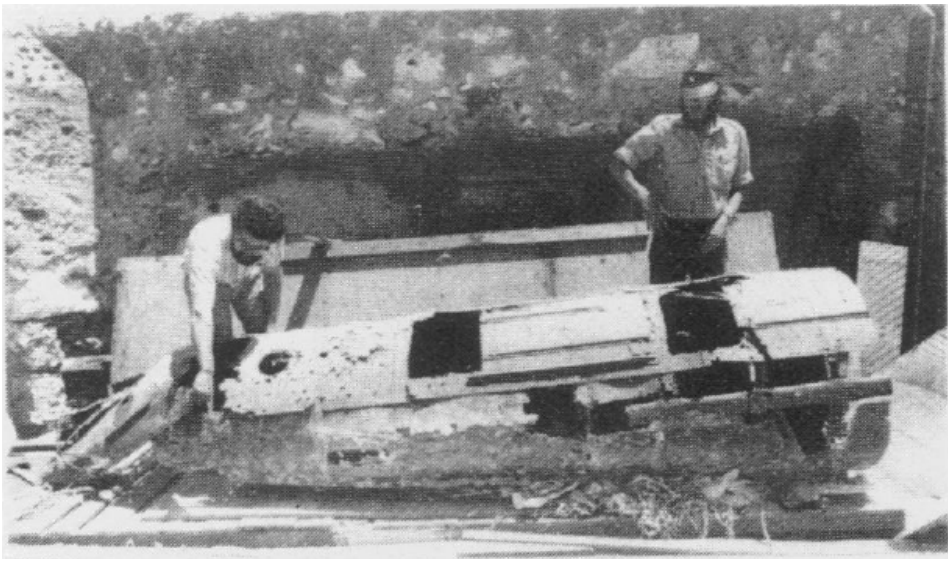

Figure 1.2 Junkers W33 aircraft in an "as received" condition, showing extensive corrosion after 46 years' exposure to salt air [4].

Deterioration of materials in seawater is due to the cumulative effect of temperature, pH, dissolved oxygen, salinity, sea current and extent of biofouling. The aluminum alloys used in the early part of the 20th century contained copper as one of the major alloying elements. Copper helps to increase the mechanical properties of aluminum alloys [6]. However, the corrosion resistance of such alloys is lower than pure metal. Copper acts as a cathode and sets up a galvanic cell with aluminum. Aluminum acts as anode and is corroded preferentially [4].

Studies regarding the methods adopted to conserve such alloys are reported in 'Stabilization of Corroded Aluminium' by Ian D. MacLeod [4]. A major part of damage to the material is seen to be caused by pitting corrosion as seen in Figure 1.3. A process is suggested to extract the chloride ions, which are the major contributors in the post-recovery corrosion [7], from the pits in the metal surface. Chloride ions can easily penetrate through the passive oxide film and cause breakdown of the passive layer [8]. The use of an ammonia-ammonium sulphate buffer at pH 9.6 in aerated deionised water effectively removes copper metal and copper corrosion products from the surface of the object while also removing aggressive chloride ions. However, the above mentioned method is only tested for aluminum alloys containing copper.

Figure 1.3 The Junker's W33 showing extensive pitting corrosion on the skin.

In 1992, Christopher D. Adams, developed a method which could be used for aircraft containing ferrous alloys and other aluminum alloys, for removing the calcareous deposits and extraction of chloride ions from the alloy surface [5]. It is indicated that the process suggested by Ian D. MacLeod [4] takes a long time, sometimes taking years, for extracting the chloride ions from an aircraft surface which was manufactured using a combination of various alloys. Christopher D. Adams recommends a more comprehensive method that can be used for combinations of ferrous and aluminum alloys. The concretion and the loose corrosion products are removed by immersing the aircraft in citric acid solution buffered with sodium hydroxide. The concretions on ferrous components are removed using basic solution which would not harm the aluminum alloys. This is followed by removal of silicates from the metal surface under tap water. The metal surface then undergoes dechlorination using cathodic

polarization. The penultimate step consisted of drying using a hot air gun. Final step consists of application of protective coatings before the artifacts goes on display.

By observing the surface of most of the previously mentioned aluminum wreckages exposed to seawater for an extended period of time, it is evident that pitting causes most of the damage to the metal as shown in Figure 1.2.

1.1 Objective of the study

1. To develop a procedure to conserve aluminum alloy 2024 belonging to the 1920 to 1950 period, in seawater environments.
2. Study the aluminum alloy 2024 for its chemical composition and mechanical properties.
3. Comparison of aluminum alloy belonging to Carnuba to modern aluminum alloys.
4. Suggest a mechanism of corrosion of the aluminum alloy 2024 in seawater.
5. Study the effect of chloride ions on the corrosion of aluminum alloy 2024.

2. MARINE CORROSION

2.1 Types of marine environment

This section presents a brief discussion regarding conditions of marine environment as such as atmosphere seawater interface, splash zone, tidal zone, shallow water, continental shelf, and deep sea and ocean bed, and their effect on metal corrosion [9]. Figure 2.1 illustrates the material loss in different zones. The actual numbers will change with the metal in consideration [9].

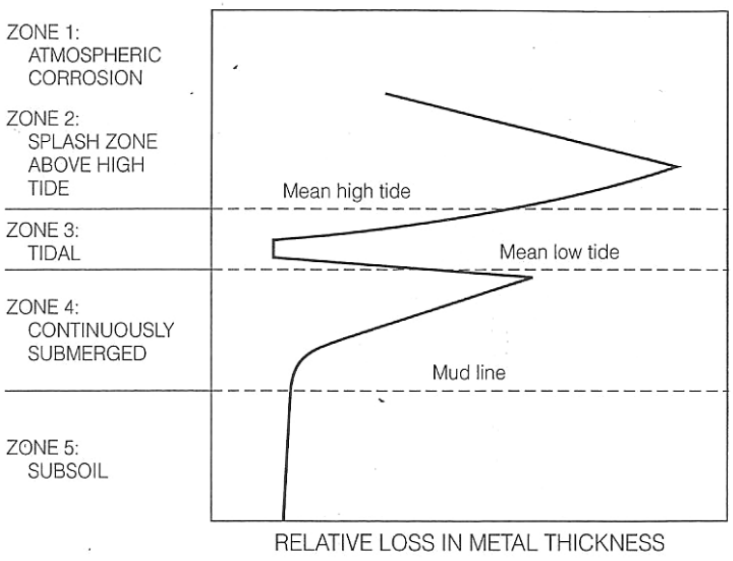

Figure 2.1 Material loss due to corrosion in various zones of the sea environment [9].

2.1.1 Atmosphere seawater interface

The atmosphere interface close to the surface of the seawater contains salt particles and has high humidity content. Figure 2.2 shows the elemental composition of seawater. The sea currents carry these salt particles. Wind velocity and direction, dew cycle, rainfall, temperature, solar radiation, dust, season and pollution directly affect corrosion. Another reason for corrosiveness in this zone is the availability of oxygen in abundance. Figure 2.1 shows the corrosion rate in this zone relative to other zones.

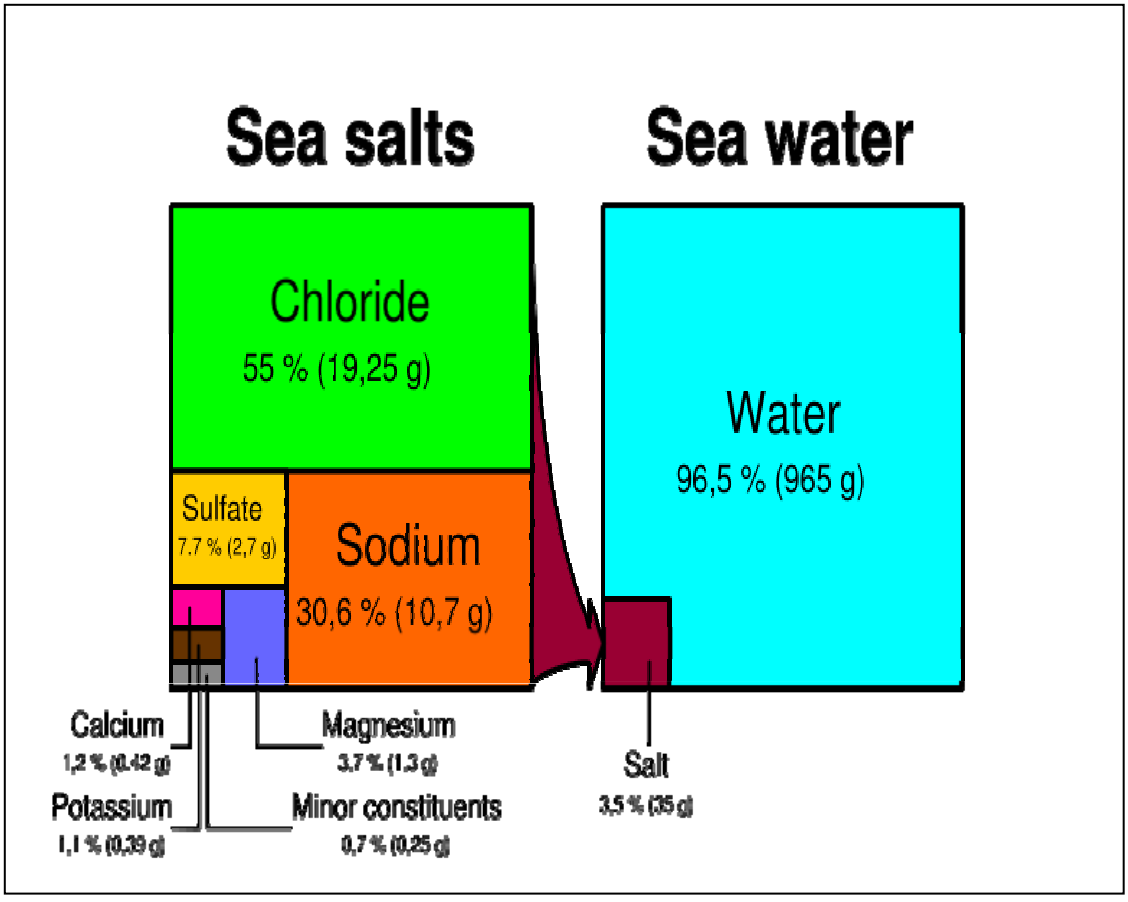

Figure 2.2 Average composition of seawater per 1000 grams of seawater[10].

2.1.2 Splash zone

The splash zone is intermittently exposed to seawater and air. This is the most aggressive zone and there is no fouling in this zone and the supply of fresh oxygen is always available.

2.1.3 Tidal zone

This zone is exposed to continuous barrage of well aerated seawater. The seawater may recede during low tides, which will leave the metal exposed to atmospheric oxygen in presence of an electrolyte and result in increased corrosion rate due to higher oxygen availability. A considerable amount of corrosion can take place in this zone because of availability of oxygen.

2.1.4 Shallow water

The temperature in this zone is higher as compared to the moderate or greater ocean depths. The depth of this zone is up to 40 meters. The seawater is saturated with oxygen because of proximity to atmospheric air [11]. Also, the turbulence helps to force the oxygen down the water column. It also consists of flora and hence has a constant supply of oxygen being produced due to photosynthesis. Fouling and velocity of seawater play a major role in the corrosion of materials. In case of metals exhibiting passive active transition, the fouling causes the depletion of oxygen and thus impedes development of the protective oxide film. In case of metals which do not have an ability to develop a protective oxide film, the velocity of seawater helps a constant supply of oxygen and increases the corrosion rate.

2.1.5 Continental shelf

Continental shelf is the zone adjoining the continental slope closer to the coast. The depth may vary up to 350 meters. This zone mainly consists of fauna as it does not have enough penetration of solar radiation for the flora to survive. The corrosion is mainly because of biofouling and the oxygen content can vary depending on the depth. Corrosion rate decreases slightly as one proceeds from the coast to the interior of this zone because the velocity of seawater near the coast is always greater, compared the seawater velocity in the interior. This causes depletion in supply of fresh oxygen in the interior as compared to the region closer to the coast [12].

2.1.6 Deep ocean or sea bed

The supply of oxygen in this zone is governed by temperature [11]. The oxygen content is usually enough for some corrosion to occur. This zone contains bacteria and the gases developed by bacterial action are NH_3, H_2S, and CH_4. The sulfate reducing bacteria often produce sulfides and are responsible for corrosion.

2.2 Factors affecting seawater corrosion

Seawater contains a variety of salts, living matter, dissolved gases and decaying flora and fauna. The effect of each on the corrosion behavior is interrelated. An independent study is not very easy. Table 2.1 is a list of various factors that affect the corrosion rate. It can be divided into chemical and physical properties.

Table 2.1 Factors affecting the rate of corrosion.

CHEMICAL PROPERTIES	PHYSICAL PROPERTIES
DISSOLVED OXYGEN	TEMPERATURE
SALINITY	PRESSURE
pH	

2.2.1 Dissolved oxygen

The amount of dissolved oxygen close to the water surface is high because of two reasons. Firstly, due to the presence of flora, oxygen production due to photosynthesis contributes significantly to the dissolved oxygen. Secondly, due to large turbulence, the atmospheric oxygen is forced down the water column. Below 40 meters there is a balance between oxygen production by photosynthesis and its consumption for survival. Below this depth the consumption for respiration is far greater than oxygen production and algae can survive but cannot grow. At greater depths the fauna continues to consume oxygen for respiration and decomposition of microbial content. But replenishment of oxygen only takes place by oxygen diffusion from top layers, which may be a slow process. Figure 2.3 shows the distribution of dissolved oxygen versus the water depth.

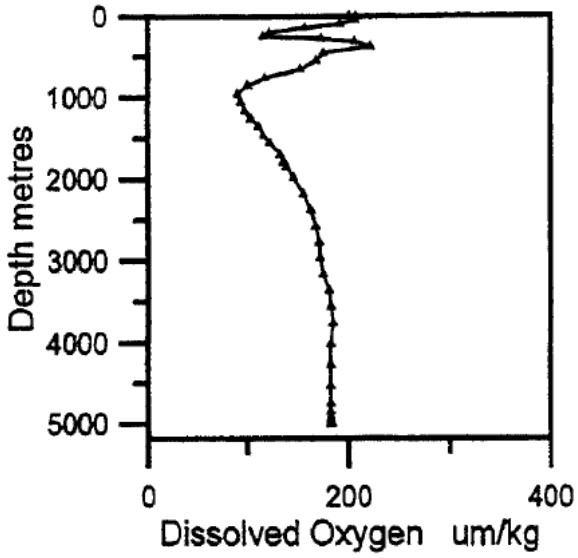

Figure 2.3 Distribution of dissolved oxygen measured against the depth of Indian Ocean [12].

Generally, a lower level of dissolved oxygen at the metal surface means a lesser probability of oxidation and hence lesser corrosion rate. The availability of oxygen thus affects the rate of corrosion. An exception to this rule would be for metals showing active passive transition. Oxygen is required to maintain and repair the passive film. Thus higher dissolved oxygen can aid in inhibiting pit initiation and growth and thus save the metal from damage. Hence, the effect of dissolved oxygen is a function of the type of metal under study and cannot be generalized for all metals. For example, stainless steel 304 will develop a protective oxide film on its surface if there is availability of oxygen and has the ability to protect itself even if a small crack develops in the oxide film [11]. A depletion of oxide film would result in bare metal surface being exposed to oxygen and seawater. This will result in corrosion of stainless steel. On the other hand, medium carbon steel will experience an exactly opposite behavior in terms

of corrosion due to amount of oxygen present. In presence of high oxygen content, the metal will oxidize and will result in loss of metal as it does not have an ability to develop a protective oxide layer on the surface. While in the presence of low oxygen content, the loss due metal oxidation will be kept in check.

2.2.2 Salinity

Salinity was defined, in 1902, as the total amount of solid material (in grams) contained in one kg of seawater when all halides had been replaced by the equivalent of chloride, when all the carbonate was converted to oxide, and when all organic matter was completely oxidized [13]. The definition of 1902 was translated into the following equation,

$$S\ (^{o}/_{oo}) = (0.03 + 1.805\ Cl)\ (^{o}/_{oo}) \quad (1)$$

where,

S is the salinity

Cl is the equivalent chlorine

The fact that the equation of 1902 gives a salinity of 0.03 $^{o}/_{oo}$ for zero equivalent chlorine was a cause for concern and a program, led by UNESCO in 1969, helped to determine a more precise relation between chlorinity and salinity was established [13]. The definition produced by the study in 1969 was,

$$S\ (^{o}/_{oo}) = 1.80655\ Cl\ (^{o}/_{oo}) \quad (2)$$

where S and Cl are as defined for equation 1.

The definition of salinity was reviewed again when techniques to determine salinity from measurements of conductivity, temperature and pressure were developed.

Since 1978, the "Practical Salinity Scale" defines salinity in terms of a conductivity ratio as,

$$S = 0.0080 - 0.1692\,K^{0.5} + 25.3853\,K + 14.0941\,K^{1.5} - 7.0261\,K^{2} + 2.7081\,K^{2.5} \quad (3)$$

where the practical salinity, symbol S, of a sample of seawater, is defined in terms of the ratio K of the electrical conductivity of a seawater sample of 15°C and the pressure of one standard atmosphere, to that of a potassium chloride (KCl) solution, in which the mass fraction of KCl is 0.0324356, at the same temperature and pressure [13]. Salinity affects two factors involved in corrosion rate, namely conductance of the electrolyte and chlorine content. The average salinity of open ocean seawater varies between 34 to 36 grams of salt content per kilogram ($^{o}/_{oo}$) of seawater. Figure 2.4 shows the variation of salinity with the ocean depth. Higher salinity increases the conductance of an electrolyte. A larger area of metal can thus participate in the corrosion reactions. In metals showing active passive transition, high conductance means a small anode and a larger cathodic area. Pitting corrosion will be the major cause of damage in this case. The second factor is chlorine content. Higher salinity means high concentration of chloride ions. Chloride ions can easily penetrate through the passive oxide film and thus cause breakdown of the passive layer [8]. The direct result of this will be initiation of a pit. Thus higher salinity can cause heavy pitting and thus damage the metal. Further sections present discussion about the effect of the chloride ion concentration on the pitting potential of the metal.

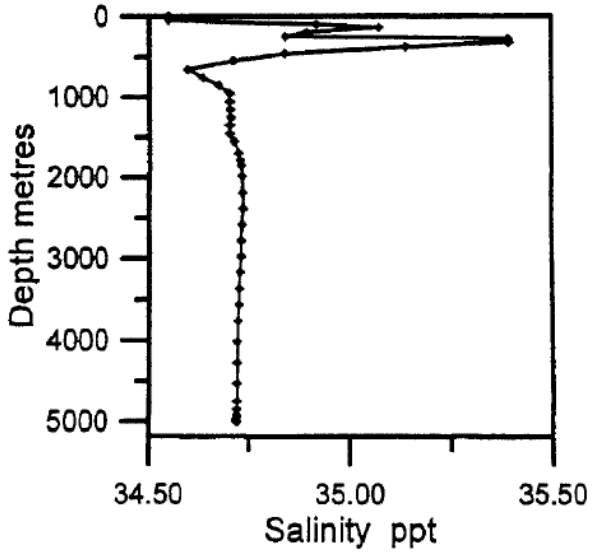

Figure 2.4 Variation of salinity with respect to ocean depth [12].

2.2.3 pH

Seawater close to the surface in contact with the atmosphere is slightly basic in nature with a pH of around 8.1-8.3. As one goes deeper into the sea due to the consumption and addition of CO_2 by the flora and fauna at different rates, the pH may reduce slightly. The range of pH for seawater is 7.7 to 8.3 [14]. Generally, variations in pH within the range 7.7-8.3 usually have no effect on the alloys used in seawater.

2.2.4 Temperature

Figure 2.5 shows the variation of temperature with respect to ocean depth. The seawater temperature decreases as we go deeper into the ocean. Biological activity increases as one goes from cold surface water in Arctic or Antarctic to tropical waters. Seawater temperature inversely affects the solubility of oxygen. Higher temperature

often means faster rate of corrosion reaction, hence a higher corrosion rate as indicated by equation 4 [11]. But it is not as simple because of the fact that dissolved oxygen is also dependent on temperature.

$$r = K\, e^{\frac{-G}{RT}} \tag{4}$$

where,

r is the reaction rate

K is the reaction rate constant

G is the activation energy

T is the temperature

R is universal gas constant

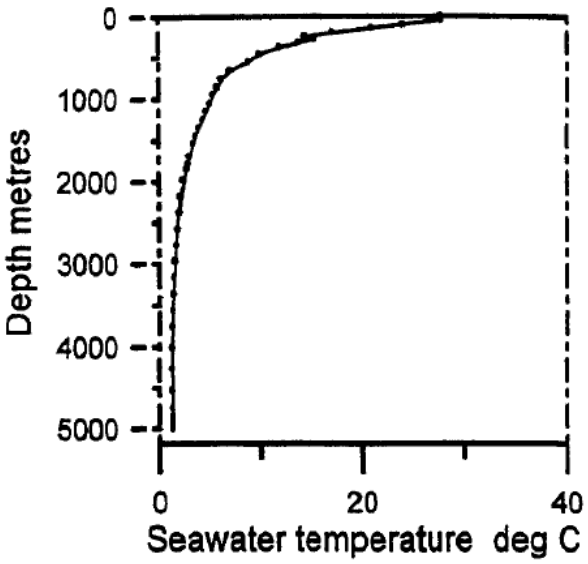

Figure 2.5 Variation of temperature with respect to ocean depth [12].

2.2.5 Pressure

There exist a direct relation between hydrostatic pressure and depth of the water column.

$$P = \rho g H \tag{5}$$

where,

P is hydrostatic pressure

ρ is density of seawater

g is acceleration due to gravity

H is the depth.

Figure 2.6 shows the linear variation of hydrostatic pressure and depth in meters.

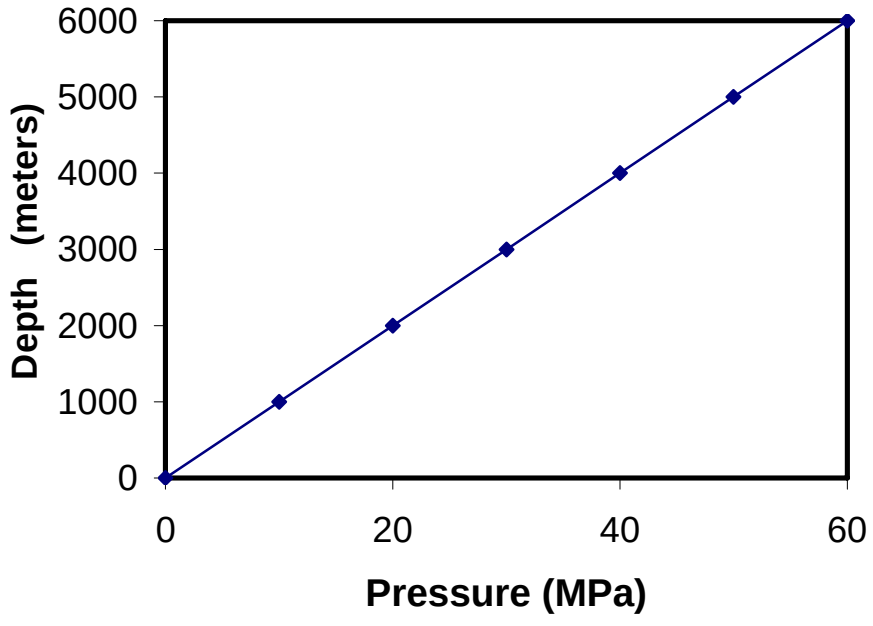

Figure 2.6 Variation of hydrostatic pressure with respect to ocean depth.

The high hydrostatic pressure near sea beds may cause a slight decrease in the ionic radius of chloride ions and it is easier for the ions to penetrate the passive oxide layer [10]. For metals displaying active passive transition, initiation of pitting is rapid due to chloride penetration.

2.3 Types of corrosion

Many different corrosion mechanisms exist. Knowledge of the most common types is well understood [11]. For each, the process is complex, incorporates many factors, and varies according to metal and specific operating conditions [15]. This section briefly discusses about some forms of corrosion with specific interest in pitting.

2.3.1 Uniform corrosion

Depiction of uniform corrosion is by corrosive attack proceeding evenly over the entire surface area, or a large fraction of the total area. General thinning takes place until failure. This is the most important form of corrosion in terms of tonnage wasted. Measurement and prediction of uniform corrosion is relatively easily, making disastrous failures rare. In many cases, it is objectionable only from an appearance standpoint. As corrosion occurs uniformly over the entire surface of the metal, it can be controlled by cathodic protection, use of coatings or paints, or simply by specifying a corrosion allowance. Thus, uniform corrosion is preferred from a technical standpoint because it is predictable and thus acceptable for design [11]. Figure 2.7 shows a uniform corrosion of part of a structure made from steel.

Figure 2.7 Uniform corrosion attack on structural steel [16].

2.3.2 Galvanic corrosion

Galvanic corrosion is an electrochemical action of two dissimilar metals in the presence of an electrolyte and a conductive path. It occurs when dissimilar metals are in contact [11]. One can depict galvanic corrosion by the presence of a buildup of corrosion at the joint between the dissimilar metals. When a galvanic couple forms, one of the metals in the couple acts as anode and corrodes faster than it would all by itself, while the other acts as cathode and corrodes slower than it would alone. One can predict the relative nobility of a material by measuring its corrosion potential. The galvanic series lists the relative nobility of certain materials in seawater. Figure 2.8 shows a general setup required for galvanic corrosion to occur. It consists of two dissimilar metals. The anode is the less noble of the two. Metal ions, called cations from the anode go into the solution or electrolyte leaving behind an electron. The driving force for this dissolution

is the potential difference between the two metals. This electron travels via the external circuit to the cathode and will be available for consumption either by the cation or other species having a net positive charge on them. The ions in the electrolyte complete the circuit. This is how the anode is consumed and corrosion takes place. Figure 2.9 shows the galvanic corrosion of aluminum in contact with a stainless steel screw.

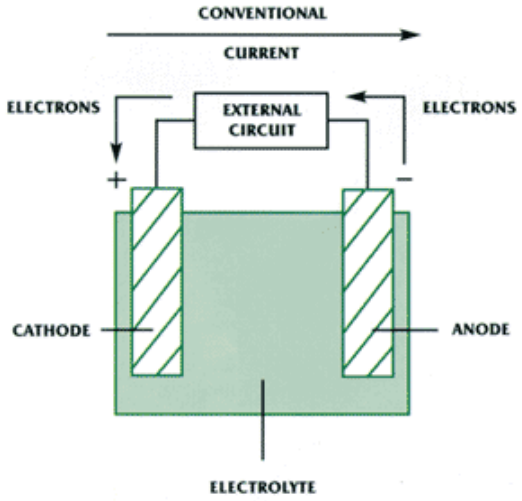

Figure 2.8 Galvanic cell with all the elements required for corrosion [17].

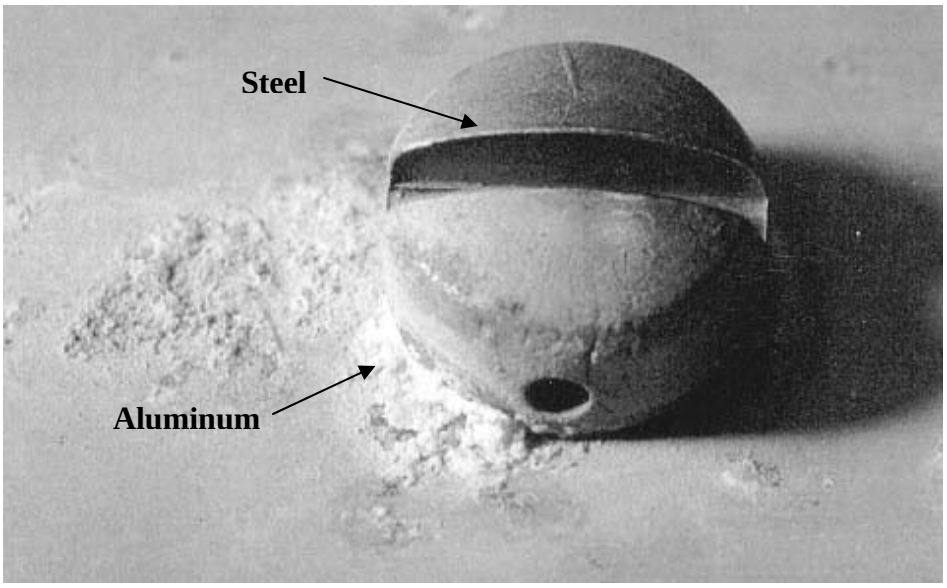

Figure 2.9 Corrosion of aluminum in contact with stainless steel screw [18].

2.3.3 Crevice corrosion

Crevice corrosion is a localized form of corrosion associated with a stagnant solution in small sheltered volumes. It occurs in localized areas such as crevices, joints, bolted and threaded parts or under existing corrosion deposits. It is the result of concentration of salts, acids and moisture, which results in the development of an occluded corrosion cell in such sheltered areas. This creates a small anode in the crevice with the remainder of the body acting as a large cathode so corrosion at the crevice is highly accelerated as well as concentrated. Deposit corrosion, contact corrosion, and gasket corrosion are terms sometimes used when a nonmetallic material forms a crevice on the metal surface [11]. Figure 2.10 depicts an example of crevice corrosion of a titanium flange.

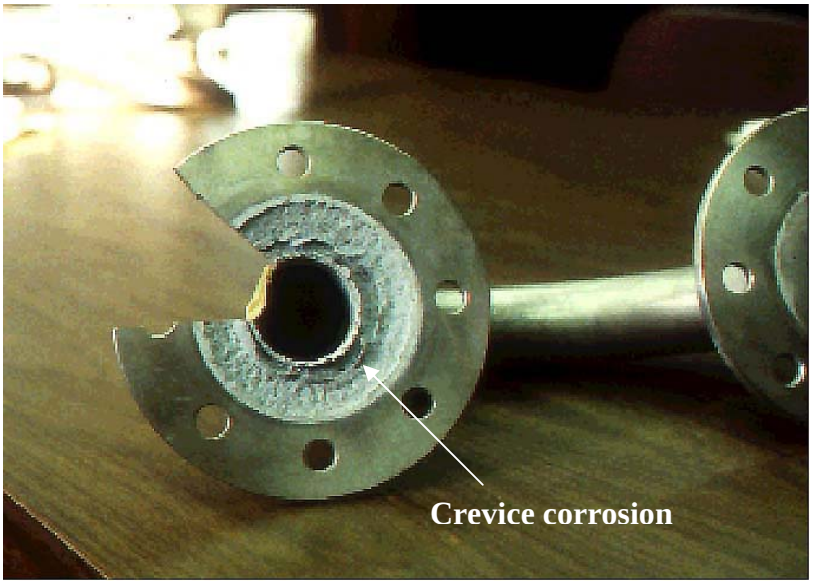

Figure 2.10 Crevice corrosion of titanium flange at an interface with a nonmetallic gasket [19].

2.3.4 Intergranular corrosion

Intergranular corrosion is localized attack along the grain boundaries, or immediately adjacent to grain boundaries, while the bulk of the grains remain largely unaffected [11]. This form of corrosion is usually associated with impurity segregation effects or specific phases precipitated on the grain boundaries. Such precipitation can produce zones of reduced corrosion resistance in the immediate vicinity. Figure 2.11 shows intergranular corrosion in a heat affected zone close to a weld. This is typical intergranular corrosion in austenitic stainless steel. Exfoliation corrosion is a form of intergranular corrosion that can exist in rolled aluminum alloys. For aluminum alloy 2024 the zone adjacent to grain boundaries depleted of copper intermetallics gets

attacked preferentially and attack occurs at the boundaries of grain elongated in the rolling direction [11]

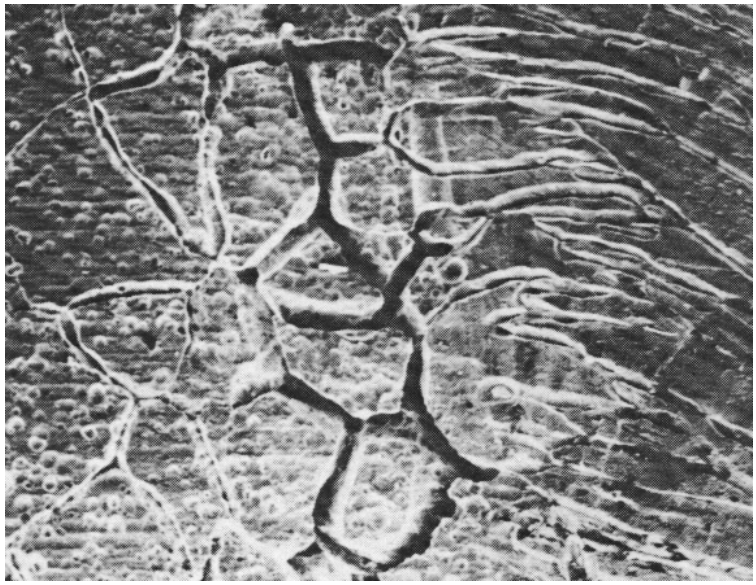

Figure 2.11 Intergranular corrosion in austenitic stainless steel [20].

2.3.5 Pitting corrosion

Pitting corrosion is a localized form of corrosion producing cavities in the material. Pitting is more dangerous than uniform corrosion damage because it is more difficult to detect, predict and design against. Corrosion products often cover the pits. A small, narrow pit with minimal overall metal loss can lead to the failure of an entire engineering system.

Pitting is initiated by localized chemical or mechanical damage to the protective oxide film. Water chemistry factors that can cause breakdown of a passive film are acidity, low dissolved oxygen concentrations and high concentrations of chloride. Localized damage or poor application of protective coatings is favorable site for pit

initiation. Other favorable sites include nonuniformities in the metal structure of the component like inclusion.

The pitting mechanism is explained using Fontana and Greene's model [21]. Figure 2.12 depicts the whole pitting process. The process consists of four stages as explained below.

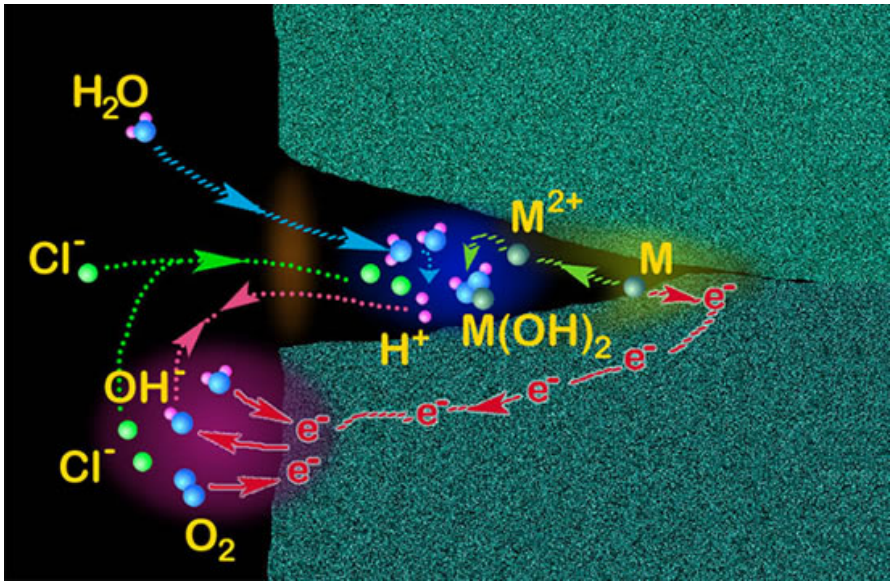

Figure 2.12 Mechanism of pitting corrosion [22].

Stage 1:

Corrosion occurs as normal both inside and outside the pit:

Anodic reaction: $M \rightarrow M^{n+} + ne^-$

Cathodic reaction: $O_2+2H_2O +4e^- \rightarrow 4OH^-$

Stage 2:

At this stage, the cathodic reaction inside the pit consumes most of the oxygen available.

Table 2.2 Conditions existing inside and outside the pit during stage 2.

Inside the pit	Outside the pit
O_2 depleted	O_2 readily available
Anodic reaction	Cathodic reaction

Stage 3:

Table 2.3 Conditions existing inside and outside the pit during stage 3.

Inside the pit	Outside the pit
O_2 depleted	O_2 readily available
Anodic reaction	Cathodic reaction
High $[M^{n+}]$ concentration	High $[OH^-]$ concentration
Overall positive	Overall negative
High $[Cl^-]$ concentration	Normal $[Cl^-]$ concentration

Cl^- and OH^- diffuse into the crevice to maintain a minimum potential energy. Metal chloride is formed. Hydrolysis of metal chloride lowers pH.

$$MCl_n + nH_2O \rightarrow M(OH)_n + nHCl$$

Stage 4:

Table 2.4 Conditions existing inside and outside the pit during stage 4.

Inside the pit	Outside the pit
Low pH	Normal pH
High $[Cl^-]$ concentration	Normal $[Cl^-]$ concentration
High $[M^{n+}]$ concentration	Low $[M^{n+}]$ concentration

More M^{n+} ions attack more Cl^- leads to lower pH inside pit. This accelerates metal dissolution and produces more M^{n+} ions, which again attack more Cl^-. This further lowers pH. If this process continues for an extended time without hindrance, the pit may run through the thickness of the material. Figure 2.13 shows a transverse section of a stainless steel tube with a pit.

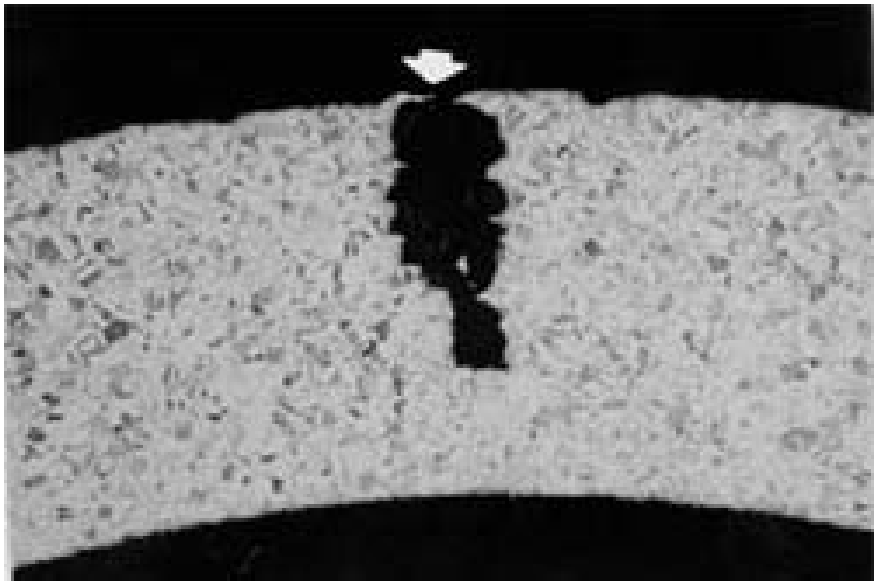

Figure 2.13 Pit growing through the thickness of a stainless steel tube [23].

2.3.6 Microbiologically induced corrosion

Microbiological corrosion (MIC) refers to corrosion and ensuing loss of metal caused by biological organisms. A number of metals, such as structural steels and copper alloys, tend to corrode generally over the entire surface in the absence of crevices or galvanic effects. In such cases, corrosion is determined by the rate at which dissolved oxygen can be delivered to the metal surface. Biological organisms present in the

aqueous medium often have the potential to increase or decrease oxygen transport to the surface; consequently, these organisms have a role in increasing or decreasing general corrosion [11]. Most MIC, however, manifests itself as localized corrosion because most organisms do not form a continuous film on the metal surface. Microscopic organisms also tend to settle on metal surfaces in the form of discrete colonies or at least discrete, rather than continuous films. Biological organisms fall under two groups based on the type of corrosion they engender: (a) anaerobic corrosion (b) aerobic corrosion. Sulfate reducing bacteria (SRB) are a typical example of anaerobic MIC. Facultative bacteria are another category of biological organisms which can cause MIC. Facultative bacteria can use either molecular (dissolved) oxygen or oxygen obtained from food material such as sulfate or nitrate ions. In other words, facultative bacteria can live under aerobic or anaerobic conditions.

When microbial deposits form on the surface of a metal, they often behave as inert deposits on the surface, shielding the area below from electrolyte. A differential aeration cell forms, even for a very small colony. The area directly under the colony will become the anode and the metallic surface just outside the contact area will support the reduction of oxygen reaction and become the cathode. Metal dissolution will occur under the microbial deposit, and resembles as pits.

In anaerobic conditions, some bacteria can reduce the sulfate ion to produce oxygen and the sulfide ion. These bacteria are called sulphate reducing bacteria (SRB). The sulfide ion then combines with ferrous ions to form iron sulfide in iron alloys. The metal surface is thus dissolved.

3. MATERIAL PREPARATION AND TESTING PROCEDURE

In order to gain a better understanding concerning the fabrication of the engineered metal alloys used to construct, repair or refurbish the Sikorsky S-38 during its working career, eight inarticulate pieces of *Carnauba* were collected on site and exported to Texas A&M University under a permit issued by the Indonesian Cultural Ministry. Figure 3.1 shows the design of a Sikorksky S-38 aircraft. Selection criteria for individual fragments included material composition, fabricated shape and the processes employed to achieve the shape, function within the structure, and availability. All pieces were kept in original condition as we did not want to disrupt structural integrity.

Two of the selected pieces were of a ferrous-based alloy and five were of an aluminum alloy. The eighth sample was selected for security reasons not for analysis. While excavating a small test pit on centerline and six feet in front of the plane, a small portion of the instrument panel was discovered with one intact instrument (except for the broken glass covering over the face), remaining affixed to the cover plate. The rationale for the object's recovery was that due to its size and interesting composition it may not remain on the site. Conservation and research would hopefully provide information concerning its manufacture.

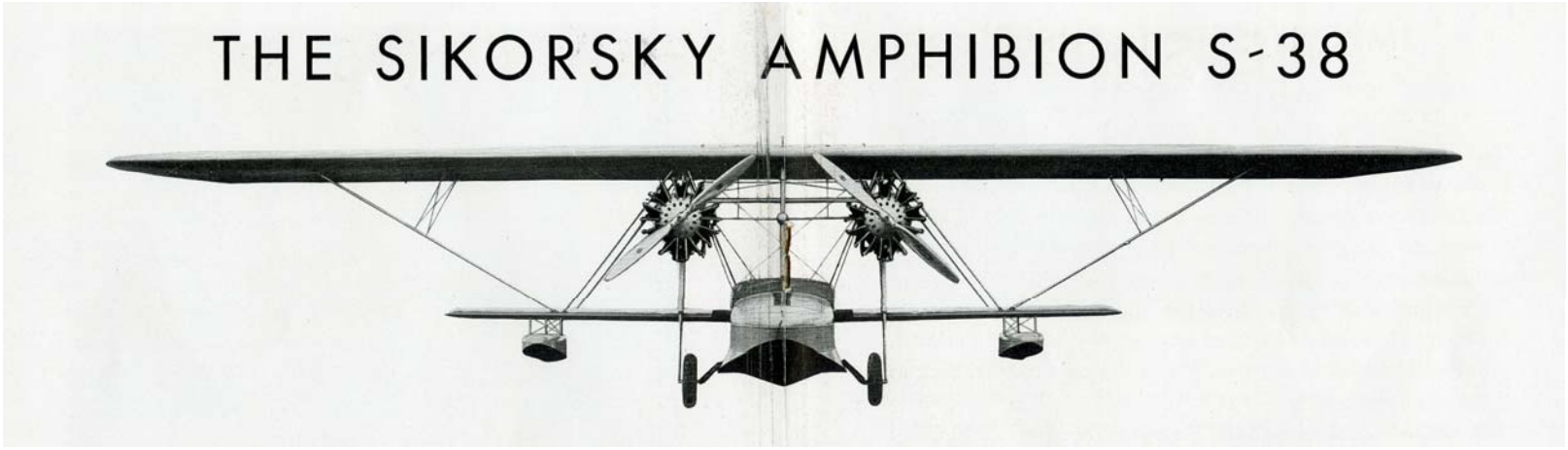

Figure 3.1 Sikorsky S-38 aircraft [24].

On site, the sample materials were photographed as shown in Figure 3.2 and its provenance recorded before collection. All samples were found in front of the aircraft or along the port wing and all but one was either lying on the surface or under a slight cover of sediment. Only the instrument (Sample #8), as already mentioned, was discovered buried in the sediment 6.5 feet off the front of the plane along the centerline.

Figure 3.2 The assemblage of the collected Carnauba samples before packaging for transport and storage.

Once on board the *Raja Ampat*, the individual samples were temporarily stored in seawater before a gentle cleaning to remove all living biomatter. Then they were measured, photographed, and written descriptions were made concerning provenance and level of preservation. This information was used to form the basis of the export permit application and to begin the scientific record of each object. After recording, the samples were sectioned in order to place them in an adequate shipping container for the

trip to Texas, stored in freshwater and refrigerated. Between the date of retrieval and departing Manokwari the water was refreshed six times.

To transport, each sample was wrapped in foam saturated in water, sealed inside plastic film, which in turn was wrapped in aluminum foil. The wrapped packages were then placed inside thermal coolers with cold packs. During extended layovers on the trip back to Texas, the samples were removed from the containers and placed back into refrigeration and the cold packs refreshed.

Once at Texas A&M, the samples were removed from their packaging and placed in purified water. Further documentation photography was undertaken and portions of the calcareous layer extracted for genomic analysis.

Eight samples belonging to *Carnauba* were collected, and seven oven-dried and brought into the laboratory. The samples were then photographed to trace back any surface details necessary after the samples had been consumed for various analyses and tests. The seven samples had been immersed in seawater for approximately 70 years and had a thick layer of calcareous material and barnacles attached to the surface. The calcareous deposits were very brittle, but strongly adhered to the surface. Barnacles attach themselves to surfaces by a cementitious secretion of insoluble polyphenolic protein complex, which acts as an excellent underwater adhesive. The combination of calcareous deposits and barnacle glue was difficult to remove and had to be subjected to a shearing force in order to disrupt the bond with the metal surface. A pneumatic scribe was used to dislodge the cementitious layers. Shear forces cause the thick layers to loosen their grip on the metal surface. The thick layer can then be chipped off easily.

After all the deposits were removed, sections of 1 cm x 1 cm were cut off from the samples using a band saw. Some of these sections were then mounted in epoxy for microstructural analysis. One section from each sample was sent for chemical analysis to A & M Technical Services Inc., Houston, TX. The main purpose of the chemical analysis was to determine the alloy composition of each sample. After placing the sectioned samples in a mold and mounting then in epoxy, they were left for natural air curing for a minimum period of 24 hours. The curing caused the epoxy to harden and it was then removed from the mold. The dimensions of the specimen obtained were 1 inch in diameter and height. This helped in gripping the specimen for polishing using silicon carbide paper. Final polishing was done using 0.3 μm size particle of alumina and 0.05 μm size particles of colloidal silica. After the final polishing, the specimen surface was etched with a solution containing 95% H_2O, 2.5% HNO_3, 1.5% HCl and 1%HF commonly known as Keller's reagent as shown in Figure 3.3.

LIGHT METALS - Aluminum and Alloys

Composition	Comments
1. 95 mL water 2.5 mL HNO_3 1.5 mL HCl 1.0 mL HF	Keller's reagent, very popular general purpose reagent for Al and Al alloys, except high-Si alloys. Immerse sample 10-20 seconds, wash in warm water. Can follow with a dip in conc. HNO_3. Outlines all common constituents, reveals grain structure in certain alloys when used by immersion.
2. 90-100 mL water 0.1-10 mL HF	General-purpose reagent. Attacks $FeAl_3$, other constituents outlined. The 0.5% concentration of HF is very popular.
3. 84 mL water 15.5 mL HNO_3 0.5 mL HF 3 g CrO_3	Graff and Sargent's etchant, for grain size of 2XXX, 3XXX, 6XXX, and 7XXX wrought alloys. Immerse specimen 20-60 seconds with mild agitation.
4. 1.8% fluoboric acid in water	Barker's anodizing method for grain structure. Use 0.5-1.5 A/in², 30-45 V dc. For most alloys and tempers, 20 seconds at 1 A/in² and 30 V dc at 20 °C is sufficient. Stirring not needed. Rinse in warm water, dry. Use polarized light; sensitive tint helpful.

Figure 3.3 Etching agents for aluminum alloys (courtesy: Buehler Ltd.) [25].

After etching the samples they were observed under the optical microscope for microstructure evaluation. Etching gave an excellent contrast between the grain boundaries and the grains themselves. The evolved microstructure was then observed under optical microscope and photographs of these microstructures were taken using a digital camera attached to the microscope. Microstructures at various magnifications were taken. Samples were then evaluated using the JEOL 6400 scanning electron microscope (SEM) for primary elemental analysis. Selected areas were checked using energy dispersive spectroscopy (EDS) to give a qualitative analysis of the chemical compositions in those areas. The analysis was then compared to the results obtained from the chemical analysis reports obtained from A&M Technical Services Inc., Houston, TX. The same samples were then used for Vickers microhardness testing. Six readings per specimen were taken and average hardness was determined. Another set of samples was prepared for evaluating the pitting potential of the aluminum alloy

belonging to aircraft. Specimens of size 1cm by 1cm were cut and a copper wire was connected to these specimens using conductive epoxy. The specimens were then mounted in epoxy with the copper wire sticking out from the side opposite to the exposed specimen surface. The metal specimens were then polished in the same manner as mentioned above and were left unetched. The polished specimens were then used to plot potentiodynamic DC corrosion plots. An electrochemical cell as shown in Figure 3.4, consisting of an electrolyte, a calomel reference electrode, a graphite counter electrode and the specimen as the working electrode were used for this purpose. A potentiostat and software supplied by GAMRY Instruments was used to plot the potentiodynamic curves. Electrolytes were prepared from sodium sulfate and sodium chloride anhydrous salts and distilled water. Various concentrations as listed in Table 3.1 were used to test the specimens.

Table 3.1 Molarities of the electrolytes used for potentiodynamic curves.

Sodium chloride concentrations in molarity	**Sodium sulfate concentrations in molarity**
0.6 M	0.03 M
1 M	1 M
2 M	
3 M	

The selection of salts was done on the basis of the two must abundant anions present in seawater as shown in Figure 2.1. Seawater contains an average of 19 grams of chloride ions and 2.71 grams of sulfate ions per kg of seawater. Other concentrations

were used to study the effect of change of concentration on corrosion resistance. The corroded samples were then evaluated using the JEOL 6400 SEM for corrosion products or any other deposits on the surface of the alloy.

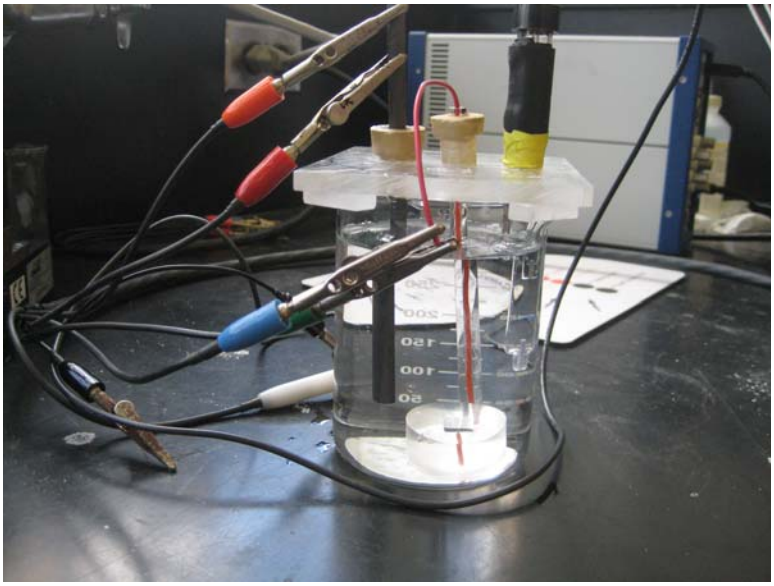

Figure 3.4 Electrochemical cell used for measuring pitting potentials.

4. RESULTS

As mentioned in Section 3, seven samples from the wreck site were brought in for evaluation and various analyses. Table 4.1 gives a summary of the procedure that was followed for testing the seven samples.

Table 4.1 Stepwise procedure for analysis of sample.

Step	Carnauba
1	Measure loss in thickness and calculate Corrosion rate
2	Polish and etch for micrographs
3	Perform chemical analysis on the samples
4	SEM and EDS analysis
5	XRD analysis
6	Plot Polarization curves for NaCl and Na_2SO_4 as a function of concentration

After cleaning all the samples, their surfaces were examines for visible corrosion damage. Areas which were not affected by corrosion were used to determine the original dimensions of the samples. The corrosion rate was determined by measuring the thickness of corroded areas. The corrosion rate was calculated by dividing the difference in the two thicknesses by the period of exposure of the component to seawater. The time taken for this reduction in the dimension was taken as 70 years. Table 4.2 gives an estimate of the life of the alloys in seawater. Average corrosion rate (column 6) was used to calculate the estimate of the life of the alloys by dividing the original thickness by the

corrosion rate. Pitting rate was calculated using the maximum pit depth observed and then dividing the maximum pit depth by 70 years.

Table 4.2 Surface analyses of seven samples recovered from wreck site and predicted life of the samples using the average corrosion rate.

Sample Number	Alloy Type	Manufacturing process	Average original thickness/ diameter (mm)	Average thickness/ diameter after corrosion (mm)	Rate of corrosion (mm/year)	Pitting rate (mm/year)	Predicted life in years
1	Aluminum 2024	rolling	3.35	1.53	0.026	0.048	129
4	Aluminum 2024	rolling	0.7	0.36	0.005	0.01	144
5	Aluminum 2024	rolling	1.6	0.9	0.01	0.023	160
6	Aluminum 2024	rolling	0.8	0.36	0.006	0.011	127
2	Aluminum 2XX	casting	2.8	1.47	0.019	0.04	147
7	Medium carbon steel	rolling	3.5	3.16	0.005	0.05	721
3	Low carbon steel	rolling	9	8.1	0.013	0.129	700

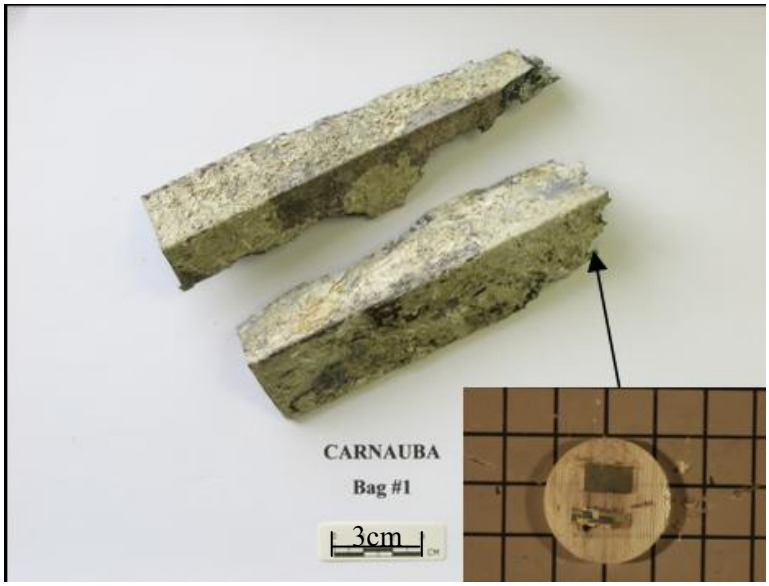

Figure 4.1 Photograph of sample 1.

4.1 Sample 1 (L channels)

Sample 1 is a part of an angle used to support the engine block as shown in Figure 4.1. The primary metal content in this alloy was aluminum with 4% copper as an alloying element. The elemental composition is as shown on page 52. If compared with the modern day alloys, its chemical composition conforms to the aluminum alloy 2024. Hardness is a measure of the resistance of a material to local plastic deformation or scratching. The average hardness value in the longitudinal direction was 157 HV (Vickers's hardness). The SEM picture shown in Figure 4.2 shows the structure within one grain. The larger bright particles are contaminants, not precipitates

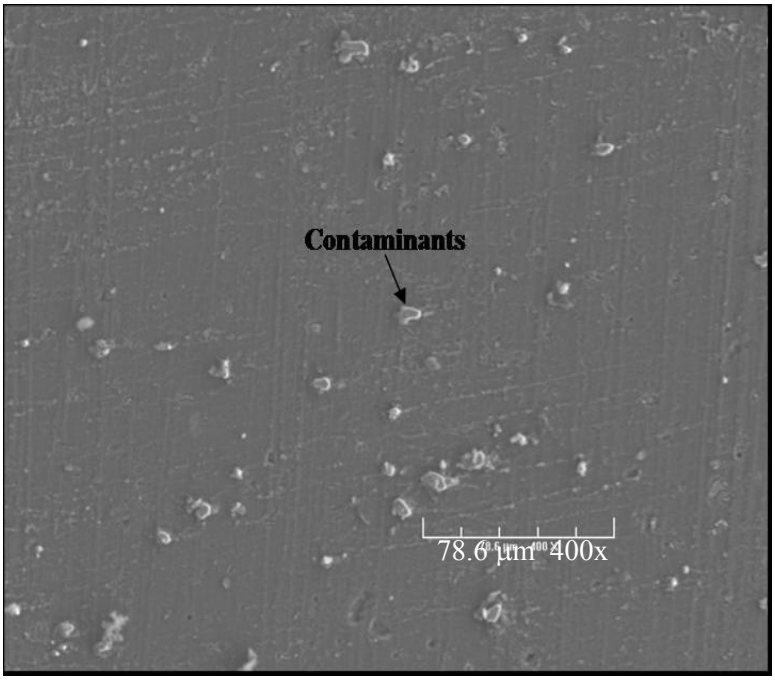

Figure 4.2 SEM photograph of sample 1.

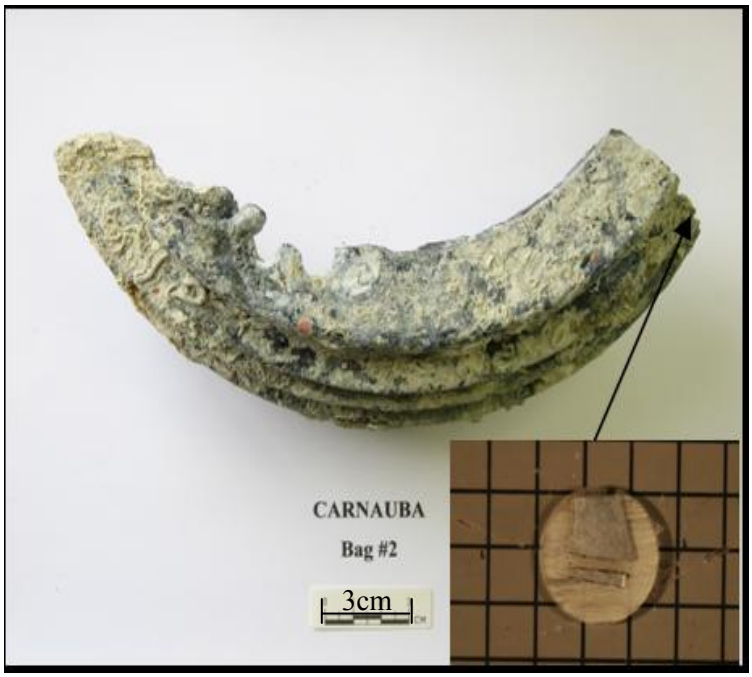

Figure 4.3 Photograph of sample 2.

4.2 Sample 2 (Part of engine cylinder with cooling fins)

This component was a part of the engine cylinder as shown in Figure 4.3. The chemical analysis shows that this is an aluminum alloy with approximately 6.5 wt% copper as the primary alloying element. The elemental composition is as shown on page 52. Due to the intricate shape of the component, the manufacturing process used was casting. This composition does not match with any of the modern day cast aluminum alloys and hence is specific to its period. The average hardness values for transverse and longitudinal direction were found to be 85 HV and 89 HV. Figure 4.4 shows a microstructure of the cast alloy. Figure 4.5 shows a microstructure of an area where exfoliation had occurred and delaminations are observed growing horizontally. The top portion of the figure shows the epoxy in which the specimen was set and the bright portion represents the metal aluminum.

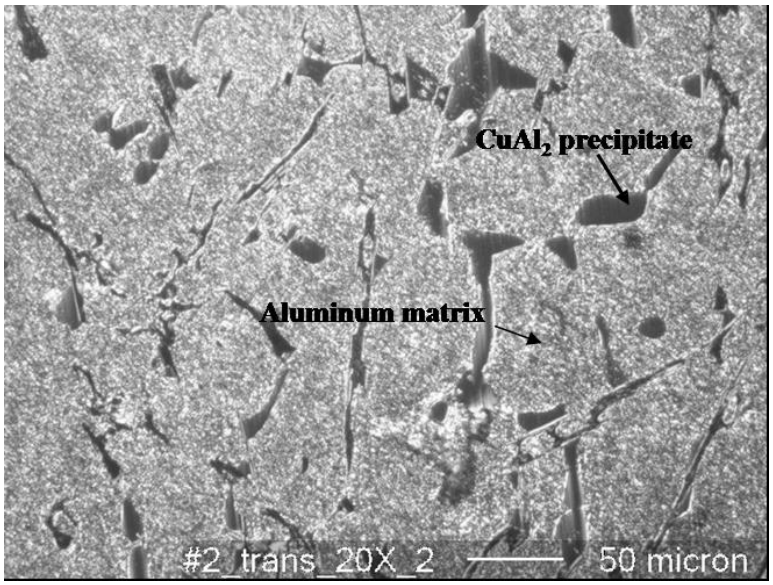

Figure 4.4 Microstructure of sample 2.

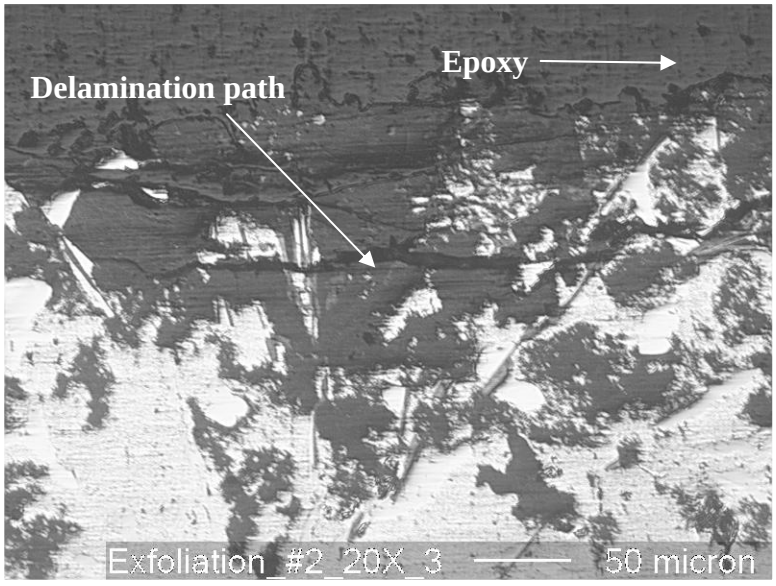

Figure 4.5 Microstructure showing exfoliation in sample 2.

The SEM photograph as shown in Figure 4.6 reveals casting defects called shrinkage, were observed in the metal.

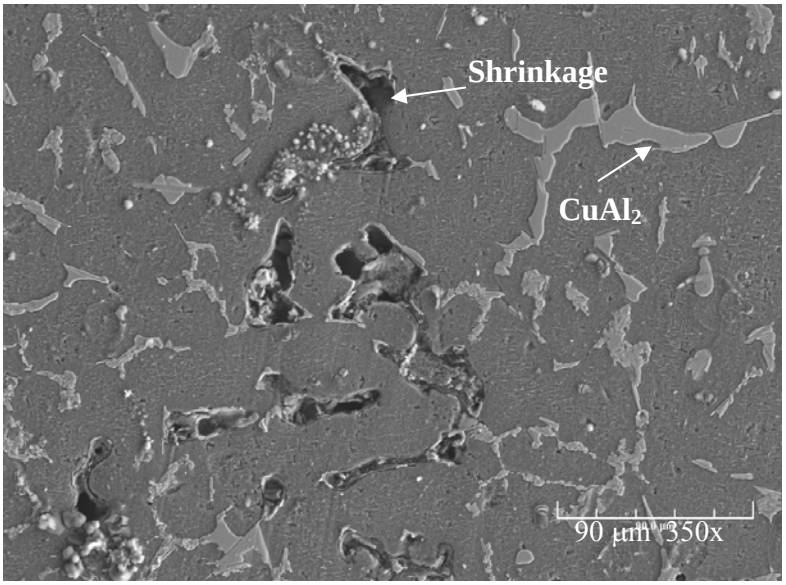

Figure 4.6 SEM photograph of sample 2 showing casting defects.

Figure 4.7 Photograph of sample 3.

4.3 Sample 3 (Actuator rod)

This component was a steel shaft which can easily be confirmed by the rust accumulated over the years as shown in Figure 4.7. The chemical composition shows a carbon percentage of 0.11%. The elemental composition is as shown on page 52. The microstructure shows a typical low carbon steel structure as indicated in Figure 4.8 with ferrite and pearlite as the main phases. The composition matches with a typical AISI 10XX series. The average value of hardness in the transverse direction was found out to be 143 HV.

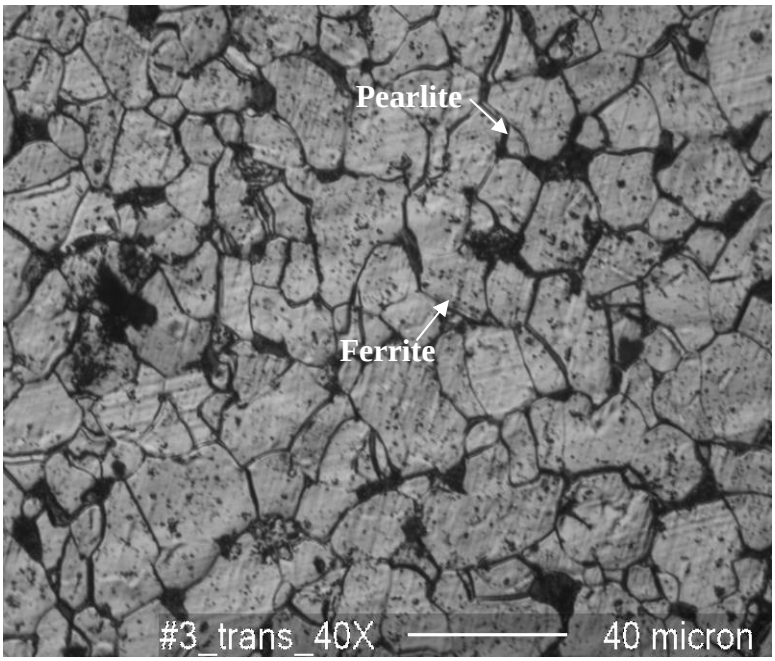

Figure 4.8 Microstructure of sample 3.

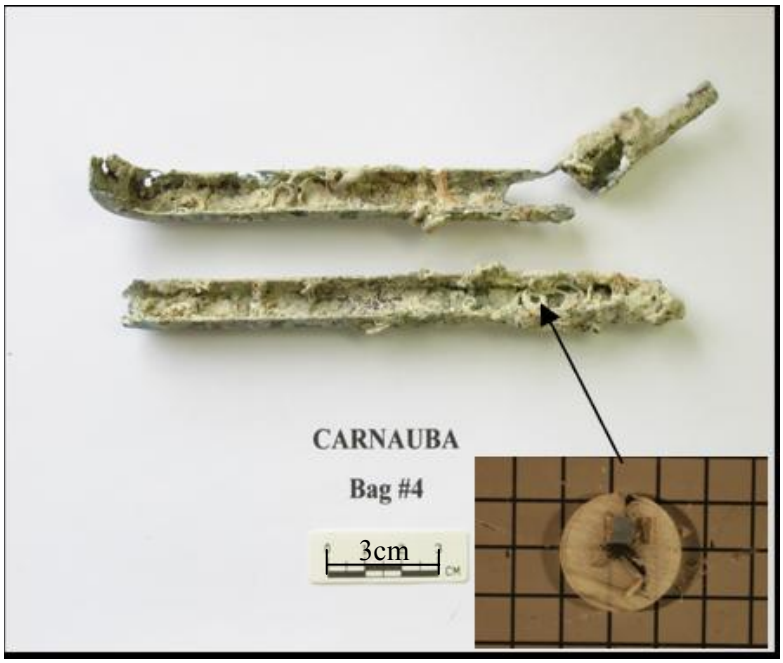

Figure 4.9Photograph of sample 4.

4.4 Sample 4 (C channels)

This component was a thin sheet of metal being bent from two sides to form a C channel as shown in Figure 4.9. The chemical analysis shows that this is an aluminum alloy with 4% copper as a major alloying element. The elemental composition is as shown on page 52. Microstructure is as shown in Figure 4.10. This alloy composition conforms to the modern day aluminum alloy 2024. The dark spots in the microstructure are copper precipitates. The average hardness values across the transverse and the longitudinal sections were found to be 160 HV and 144 HV respectively. The SEM image shown in Figure 4.11 shows some etch pits and should not be mistaken for precipitates.

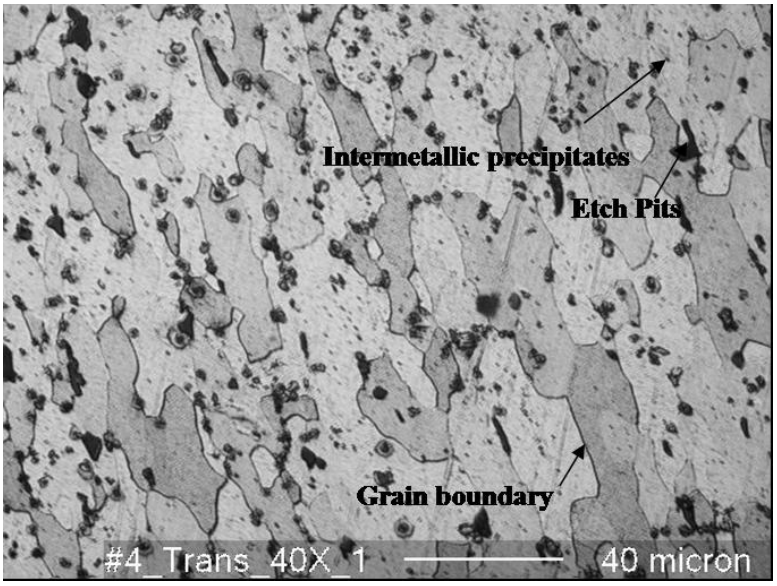

Figure 4.10 Microstructure of sample 4.

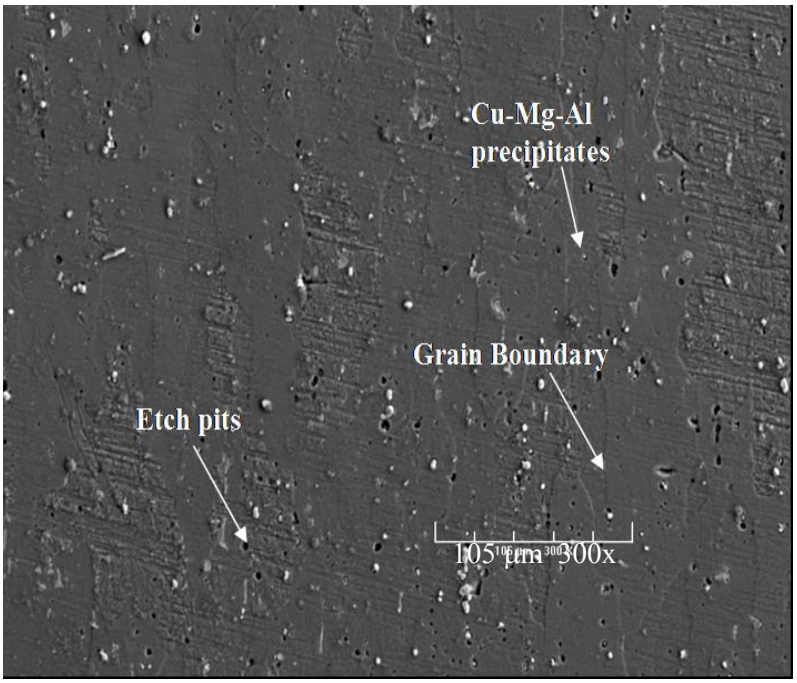

Figure 4.11 *SEM photograph of sample 4 showing Cu-Mg-Al precipitates.*

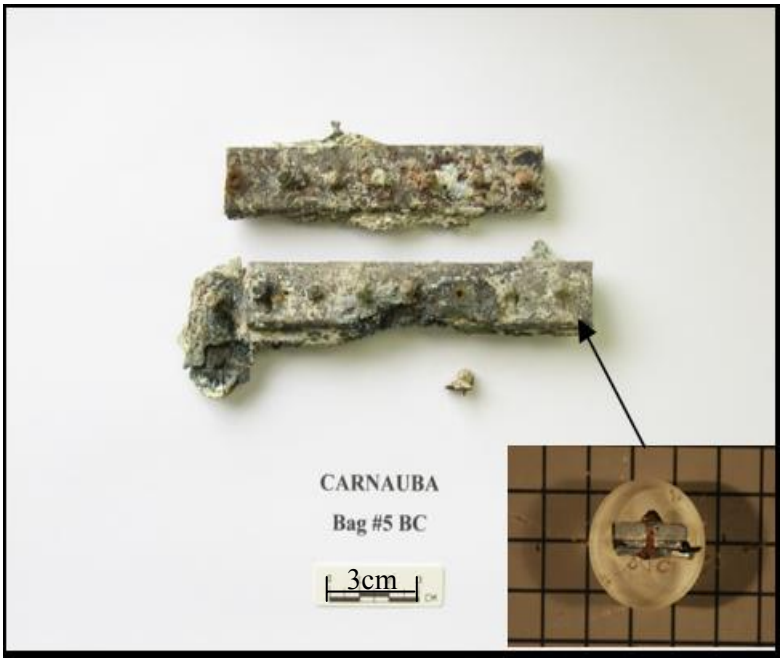

Figure 4.12 *Photograph of sample 5.*

4.5 Sample 5 (T piece)

This component was a part of a "T" piece as shown in Figure 4.12. The cross section of this component shows that it is a composite of three sheets. The chemical composition of all the three sheets shows 3.5% copper as a primary alloying element. The elemental composition is as shown on page 52. The elemental composition of this material matches with modern day aluminum alloy 2017. Figure 4.13 shows the microstructure of the alloy. The average hardness value across the transverse direction was found to be 143 HV.

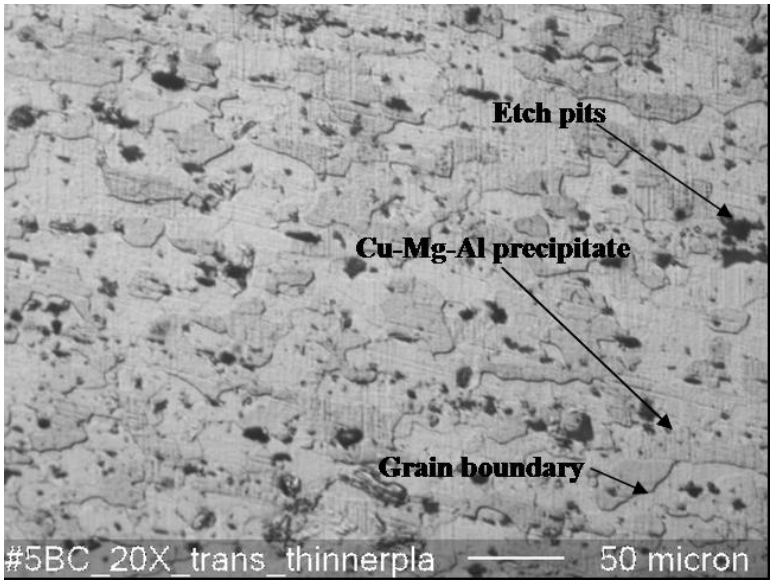

Figure 4.13 Microstructure for sample 5.

Figure 4.14 Photograph of sample 6.

4.6 Sample 6 (Skin)

This piece of metal was a thin sheet with a pit density of more than 50% as seen in Figure 4.14. The chemical analysis shows that it is an aluminum alloy with 4% copper as the primary alloying element. The elemental composition is as shown on page 52. Again the dark spots observed are the copper precipitates and inclusions. Figure 4.15 shows the microstructure. The chemical composition matches with the modern day 2024 aluminum alloy.

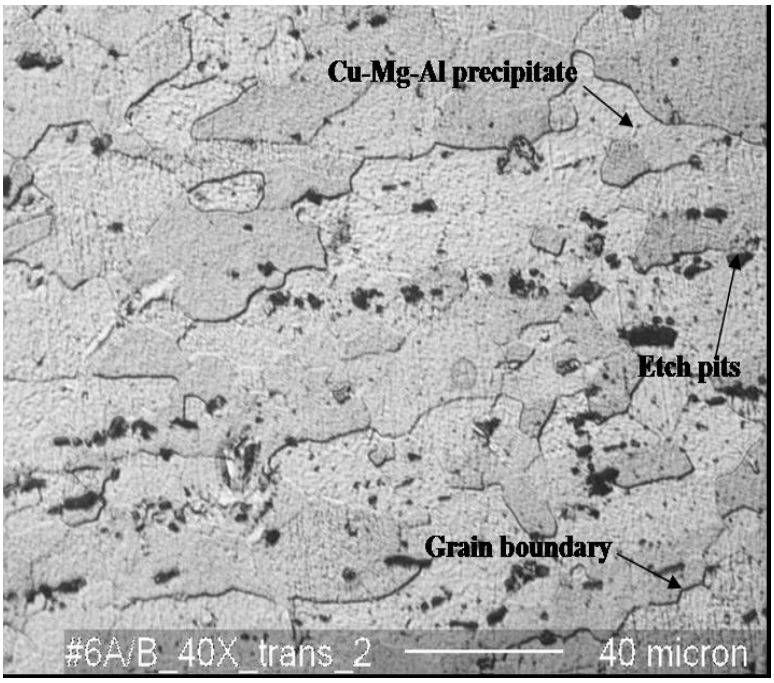

Figure 4.15 *Microstructure of sample 6.*

Figure 4.16 *Photograph of sample 7.*

4.7 Sample 7 (Cross rods)

The slender long rod shown in Figure 4.16 was one of the cross rod providing support to the wings. The chemical composition shows that it is a hypoeutectoid steel with 0.6% carbon. The elemental composition is as shown on page 52. The average values of hardness in transverse and longitudinal directions are 281 HV and 320 HV which is equivalent to 28 HRC to 30HRC respectively. Figure 4.17 shows a presence of pearlite, in which alternate layers of ferrite and cementite can be seen.

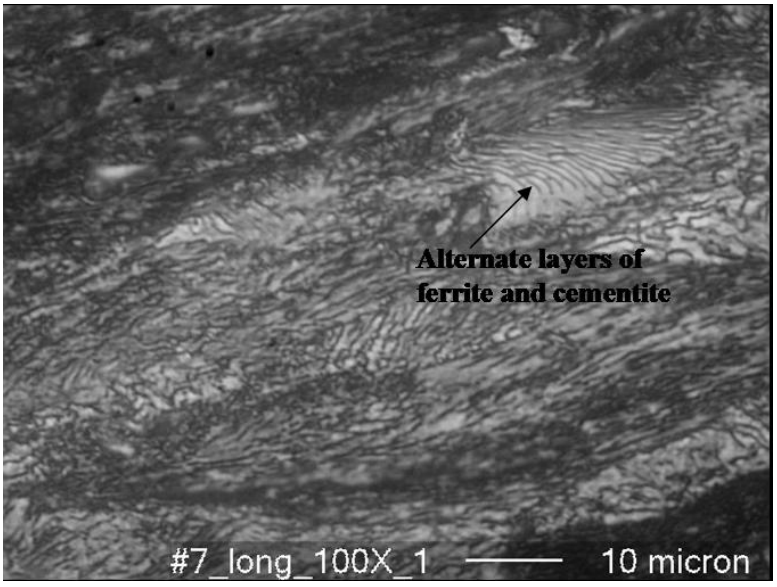

Figure 4.17 Microstructure of sample 7.

Table 4.3 shows the hardness values recorded for the seven samples. The values of above mentioned wrought aluminum alloys conform well to the modern day industrial standard values of 130 to 150 HV for a rolled and then solution heat treated with temper designation T3. T3 designation refers to heating the alloys to a solution heat treatment temperature of 525°C, soaking time depending upon the thickness, and then quenching in water at room temperature. The delay in quenching should not be more than 10 seconds [26]. Lastly the alloys undergo cold working before the final ageing process. All the seven samples were sent to A&M technical services, Houston, TX to check for the chemical composition. The elemental composition of each sample is as shown in Table 4.4. Photoemissive spectroscopy was used for this purpose and the error limits reported were 3%. The composition would help in comparison of the 1930s alloys with the modern day alloy composition.

Table 4.3 Hardness values for the samples recovered from seawater.

	Aluminum wrought samples					Cast aluminum		Steels		
	Sample#1		Sample#4		Sample#5	Sample#2		Sample#3	Sample#7	
	Hardness HV		Hardness HV		Hardness HV	Hardness HV		Hardness HV	Hardness HV	
Reading	Transverse	Longitudinal	Transverse	Longitudinal	Transverse	Transverse	Longitudinal	Transverse	Transverse	Longitudinal
1	133	160	179	131	121	94	89	149	298	300
2	158	140	188	173	153	84	92	123	265	319
3	136	160	132	133	144	77	85	161	269	309
4	129	149	142	146	141	89	87	150	282	334
5	141	177	159	139	160	81	93	134	292	340
Average	140	157	160	144	144	85	89	143	281	320
Standard deviation	11	14	24	17	14	7	3	15	14	17

Table 4.4 Chemical analysis for the seven samples from the S-38 Carnauba.

	Aluminum alloys							Steels		
	Sample 1	Sample 2	Sample 4	Sample 5A	Sample 5BC	Sample 6	2024		Sample 3	Sample 7
Element								Element		
Aluminum	93.926	91.014	93.98	94.597	94.316	94.316	93.853	Iron	98.6055	98.245
Silicon	0.36	0.63	0.47	0.34	0.36	0.36	0.1	Carbon	0.1	0.6
Iron	0.48	1.38	0.46	0.4	0.41	0.41	0.17	Manganese	0.46	0.65
Copper	4.05	6.65	3.86	3.46	3.63	3.63	3.83	Phosphorus	0.064	0.032
Manganese	0.65	0.02	0.66	0.56	0.58	0.58	0.78	Sulfur	0.072	0.03
Magnesium	0.42	0.16	0.45	0.46	0.51	0.51	1.08	Silicon	0.23	0.17
Chromium	0.01	0.02	0.01	0.08	0.09	0.09	0.01	Nickel	0.08	0.04
Nickel	0.01	0.03	0.02	0.01	0.01	0.01	0.02	Molybdenum	0.01	0.01
Zinc	0.031	0.028	0.025	0.032	0.033	0.033	0.09	Chromium	0.04	0.06
Titanium	0.008	0.012	0.01	0.006	0.006	0.006	0.012	Copper	0.23	0.06
Lead	0.005	0.005	0.005	0.005	0.005	0.005	0.005	Aluminum	0.012	0.01
Tin	0.005	0.006	0.005	0.005	0.005	0.005	0.005	Vanadium	0.002	0.002
Bismuth	0.005	0.005	0.005	0.005	0.005	0.005	0.005	Titanium	0.002	0.002
Zirconium	0.01	0.01	0.01	0.01	0.01	0.01	0.01	Niobium	0.002	0.002
Vanadium	0.01	0.01	0.01	0.01	0.01	0.01	0.01	Cobalt	0.015	0.05
Arsenic	0.005	0.005	0.005	0.005	0.005	0.005	0.005	Boron	0.0005	0.005
Boron	0.005	0.005	0.005	0.005	0.005	0.005	0.005	Tungsten	0.01	0.01
Cobalt	0.01	0.01	0.01	0.01	0.01	0.01	0.01	Zirconium	0.01	0.01
								Lead	0.005	0.005
								Tin	0.05	0.007

4.8 DC polarization measurements

Figure 4.18 shows potentiodynamic plots for aluminum alloys recovered from *Carnauba* and also the modern day aluminum alloy 2024. Chloride ions and sulphate ions being the most prevalent anions present in seawater, sodium chloride and sodium sulfate were used as electrolytes. The concentrations used were 0.6M, 1M, 2M, 3M. Sodium sulfate solution of concentration 1M was also used to check the aggressiveness of SO_4^{2-} ions. The pitting potential of around -600mV was recorded for samples which were tested using sodium chloride. The actual values of the pitting potentials are as shown in Table 4.5. Change in concentration of sodium chloride did not cause a significant change in the pitting potentials. No pitting was observed when sodium sulfate solution was used. The modern day aluminum alloy 2024 recorded the least corrosion rate while the cast aluminum alloy belonging to *Carnauba* recorded the highest. The average corrosion rate for *Carnauba* samples was 0.05 mm/year. From Figure 4.18, the average value of corrosion current observed is 4 μA and the corrosion rate is calculated as follows [11],

$$r = 0.0039\frac{E_q i}{D} \tag{6}$$

where,

r is the corrosion rate in mm/year

E_q is the equivalent weight of the alloy

D is the density in gms/cm^3

i is the current density in μA

Table 4.5 Pitting potentials for aluminum alloy 2024 with sodium chloride and sodium sulfate used as electrolytes.

Sample	Electrolyte used	Concentration (M)	Pitting potential (mV)
Carnauba 2024	Sodium chloride	0.6	-585
Carnauba 2024	Sodium chloride	1	-598
Carnauba 2024	Sodium chloride	2	-645
Carnauba 2024	Sodium chloride	3	-647
Carnauba 2024	Sodium sulfate	1	No pitting
Modern Day 2024	Sodium chloride	0.6	-570
Carnauba Cast Aluminum	Sodium chloride	0.6	-650

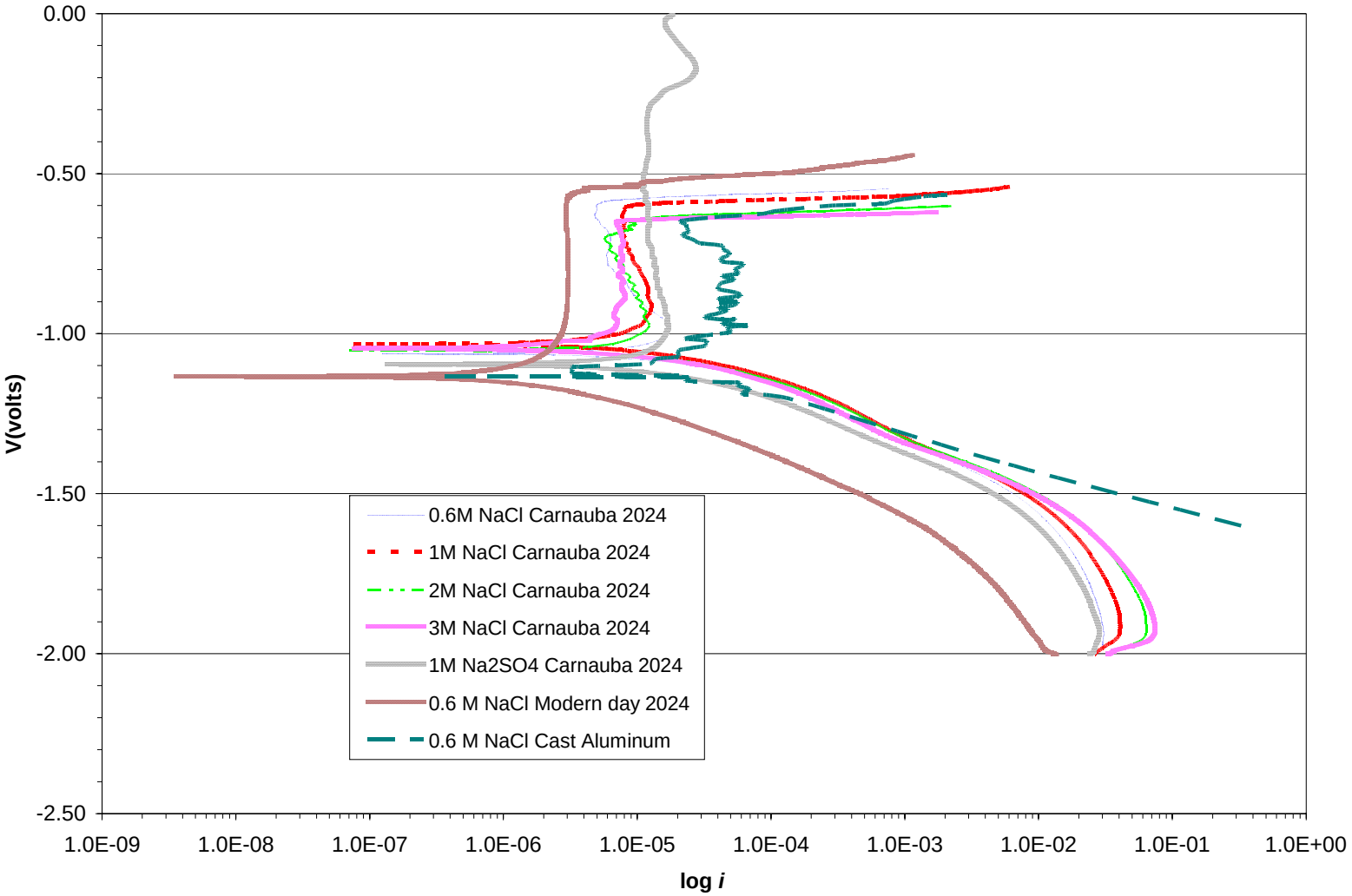

Figure 4.18 Potentiodynamic plots for aluminum alloy 2024 with sodium chloride and sodium sulfate used as electrolytes.

5. DISCUSSION

5.1 Comparison of alloy microstructure and properties for the seven recovered components

Heat treatment to increase strength of aluminum alloys is a three-step process:

1. Solution heat treatment: dissolution of soluble phases
2. Quenching: development of supersaturation
3. Age hardening: precipitation of solute atoms either at room temperature (natural aging) or elevated temperature (artificial aging or precipitation heat treatment)

The microstructure analysis of the sample shown in Figure 4.2 revealed a grain size of more than 200 μm in width and thickness. The recrystallization temperature of aluminum alloy 2024 is close to 600°F, the actual value depending upon the amount of working the material has undergone [27]. One of the initial assessments of this effect is that this piece of material could be located in a high temperature zone, such as in close proximity to the engine, which in turn could have resulted in grain growth. A larger grain size generally decreases the rate of corrosion [28]. The manufacturing process used for this component may have been rolling into sheets and then bending to form a 90° angle followed by T3 heat treatment.

The microstructure seen in Figure 4.4 reveals a cast structure. The grains are equiaxed and have an ASTM grain size of 6. The copper on solidifying forms a network at the grain boundary as eutectic of aluminum alloy 2024 is rich in copper and is the last to solidify. Due to the intricate shape of the fins and the cylinder, the manufacturing

process used to fabricate this component was casting. Cast aluminum alloys containing copper are heat treatable. Heat treatable castings have high strength, show low ductility and have good wear resistance due to presence of copper. One drawback, however, of having copper as one of the major alloying elements is that the corrosion resistance of the material is decreased and the metal becomes susceptible to localized galvanic corrosion in the appropriate environment. Copper also helps to improve the machinability of the casting [29]. Silicon is used to improve the fluidity of cast materials [29]. An interesting observation on this sample was the existence of exfoliation at the fractured boundary surface of the sample. Exfoliation is a phenomenon by which a layered effect is observed. It is normally associated with cold worked materials and not cast materials. Careful examination of the microstructure shows that the separation between the layers does not take place at the grain boundary but through the grains as shown in Figure 5.1. This is not typical of an exfoliation phenomenon.

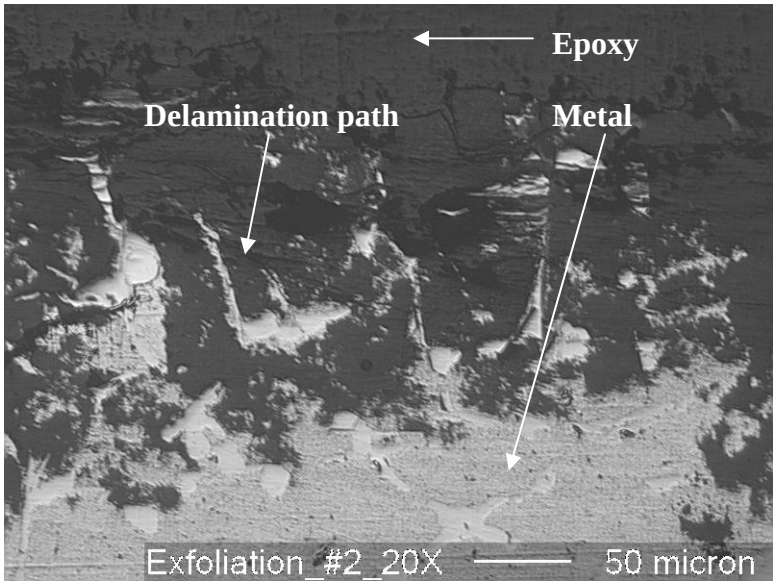

Figure 5.1 Exfoliation in sample 2.

The microstructure seen in Figure 4.8 shows a very large amount of ferrite and the elemental composition shown on page 52 shows carbon content of 0.1%, hence is a low carbon steel. The grains are mainly ferrite and seem to be annealed, which is indicated by the low hardness value of 73 HRB. The ASTM grain size measured is 8. The manufacturing process used for this component would have been rolling into thin bars, and then followed by heat treatment. Mild steel is the most common steel used in many applications as it provides sufficient mechanical properties at very low cost. It is malleable at high temperatures and hence can be forged. When strength is not a major criterion, low carbon steels are preferred over other steels due to their workability. If steel is kept in contact with an aluminum alloy in presence of an electrolyte the aluminum will undergo corrosion and steel will be protected.

The microstructure seen in Figure 4.10 reveals that the material is worked, evident from the elongation of the grains in the direction of rolling, and then solution heat treated to temper designation T3. The rolling causes highly stressed regions at the grain boundaries and grain boundaries may become anodic with respect to the matrix. This material hardens with natural or artificial aging. The manufacturing process used was rolling and then bending followed by T3 heat treatment.

The microstructure in Figure 4.13 reveals deformation in the direction of rolling. The dark spots are mainly copper precipitates and other metallic and nonmetallic inclusions. The process used to manufacture this component was rolling into thin sheets followed by T3 heat treatment. This material is similar to the other aluminum alloys mentioned earlier except for its copper content, which goes down from 4% to 3.5%.

The microstructure in Figure 4.15 shows that the grains are elongated along the direction of rolling. Heavily distorted grains may cause decrease in corrosion resistance. The manufacturing process used for this component would be rolling followed by T3 heat treatment for increasing strength and hardness. The “swiss cheese” effect seen on the sheet of metal may be due to the differential aeration caused by the barnacles attaching themselves to the metal surface. The area around the barnacles has a greater access to oxygen than the area where the barnacles have attached themselves to the metal surface. This causes a crevice effect and accelerates corrosion. The corrosion consumes dissolved oxygen in the small volume of the crevice, impairing passivity and increasing the concentration of metal cations, which attract negatively charged cations such as Cl^-. The crevice thus serves as a ready made site for localized corrosion [11].

The microstructure in Figure 4.17 shows a typical pearlitic region with alternate bands of ferrite and cementite. The direction of deformation is the direction in which the grains are stretched. The manufacturing process used is drawing into small bars. These alloys are normalized and are used in applications which require very high strength.

5.2 Corrosion mechanism of aluminum alloy 2024 in seawater

Copper distribution in alloy 2024 is inhomogeneous in nature due to the inconsistent size distribution. This can be seen by the EDS analysis conducted on the samples which underwent pitting corrosion when exposed to sodium chloride solution as shown in Section 4. Copper exists as an intermetallic compound particle or second phase particle in alloy 2024. These intermetallics are of varied sizes and are randomly distributed showing no pattern, and hence the inhomogeneous distribution. One of the compound particles is Al_2CuMg and the other is a complex intermetallic of Al-Cu-Fe-Mn. The principal compositions for the second type of intermetallic are (Cu, Fe, Mn) Al_6 and Cu_2FeAl_2 [30]. The SEM photograph of the microstructure in Figure 5.2 and EDS analysis shown in Figure 5.3 confirm the presence of Al_2CuMg intermetallics. The two intermetallics are responsible for pitting corrosion of aluminum alloy 2024. Minute flaws in the oxide film can exist at the intermetallic sites and potential differences exist between the intermetallics and the aluminum matrix. A potential difference of 200 to 300 mV exists between the intermetallics and the surrounding aluminum matrix [31]. The existence minute flaws in the protective oxide layer and the galvanic couple formed between the intermetallic and the adjoining aluminum matrix would result in localized

attack and augment the susceptibility of aluminum alloy 2024 to pitting corrosion when the alloy is exposed to solutions containing chloride ions.

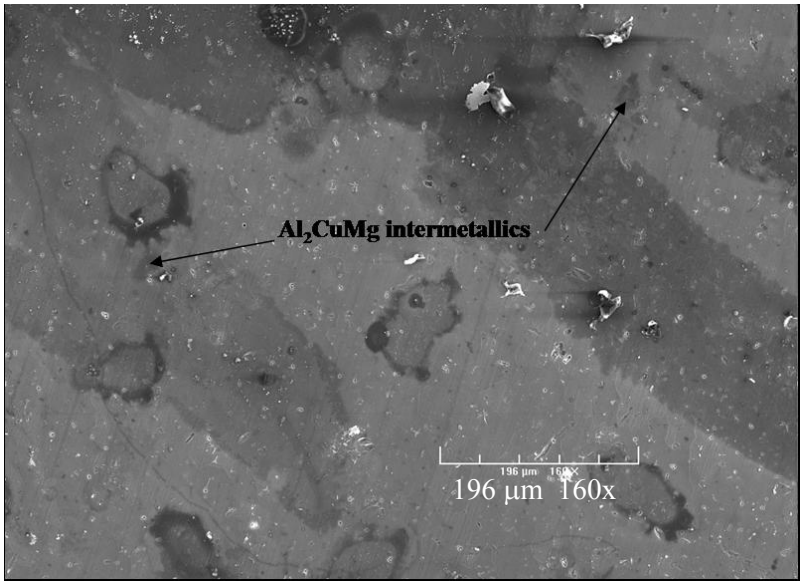

Figure 5.2 Intermetallics in aluminum alloy 2024.

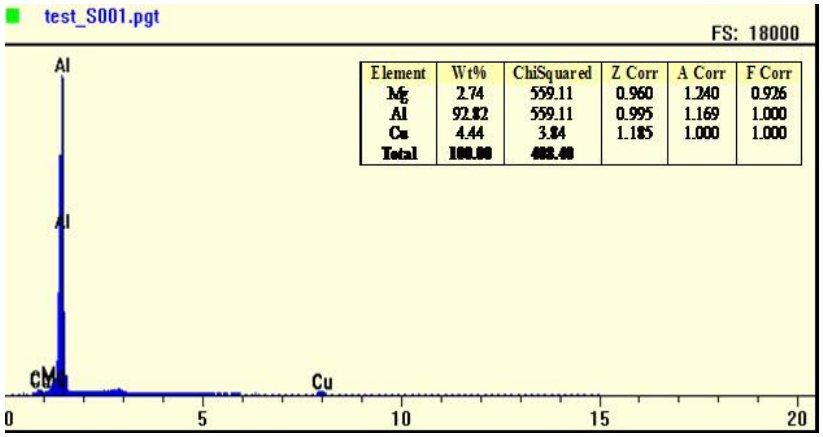

Figure 5.3 EDS analysis at the intermetallics in aluminum alloy 2024.

Initiation of pitting starts with heterogeneous adsorption of aggressive chloride ions on the surface [7]. The chloride ions seem to be preferentially adsorbed at the sites which are rich in intermetallics [7]. The adsorbed chloride ions react with aluminum and thinning of aluminum oxide by local dissolution takes place until the surface metal is exposed to the seawater solution. The pH is increased because of release of H^+ ions in this reaction and conditions become favorable for pitting. Eventually, pitting corrosion will occur. The reaction that take place between aluminum in the oxide film and adsorbed chloride ions are discussed below. The symbol H^+ indicates the presence of a hydrogen ion, but in practicality the H^+ ion attaches itself to the water molecule and is called the hydronium ion, having a chemical formula H_3O^+

$$Al^{3+} + H_2O \rightarrow H^+ + Al(OH)^{2+}$$

$$Al(OH)^{2+} + Cl^- \rightarrow Al(OH)Cl^+$$

$$Al(OH)Cl^+ + H_2O \rightarrow Al(OH)_2Cl + H^+$$

After initiation of the pit, the solution comes in contact with the copper intermetallics and because of the low pH, copper undergoes oxidation forming cuprous oxide Cu_2O. At the same time aluminum will also oxidize forming aluminum oxide Al_2O_3. Pourbaix diagrams are like phase diagrams for corrosion scientists. They are often used to give the thermodynamically most stable form of that element at a given potential and pH condition. Looking at Figure 5.4, three regions: corrosion, passivation, and immunity, can exist depending on the potential and the pH. In regions where Al^{3+} is stable, corrosion is possible, aluminum oxide is stable, resistance or passivity is possible and where Al is stable, it is thermodynamically immune to corrosion.

Various lines on the Pourbaix diagram can be interpreted in the following manner,

1. Vertical lines separate species that are in acid-base equilibrium.
2. Non vertical lines separate species related by redox equilibrium.
3. Horizontal lines separate species in redox equilibrium not involving hydrogen or hydroxide ions.
4. Diagonal boundaries separate species in redox equilibrium in which hydroxide or hydrogen ions are involved.
5. Dashed lines enclose the practical region of stability of the water solvent to oxidation or reduction.

For example, from Figure 5.5, at pH of 9 and potential of 0.0 volts we can see that Cu_2O is stable. Examination of Pourbaix diagram shows that in seawater conditions, copper corrosion products cannot exist in equilibrium with aluminum [3]. Pourbaix diagrams for aluminum and copper are shown in Figures 5.4 and 5.5.

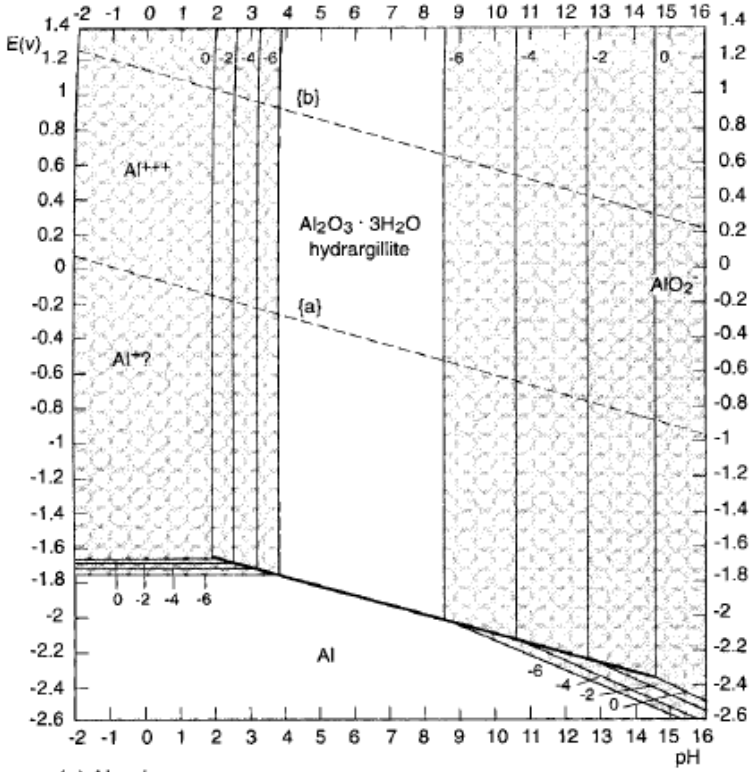

Figure 5.4 Pourbaix diagram for aluminum.

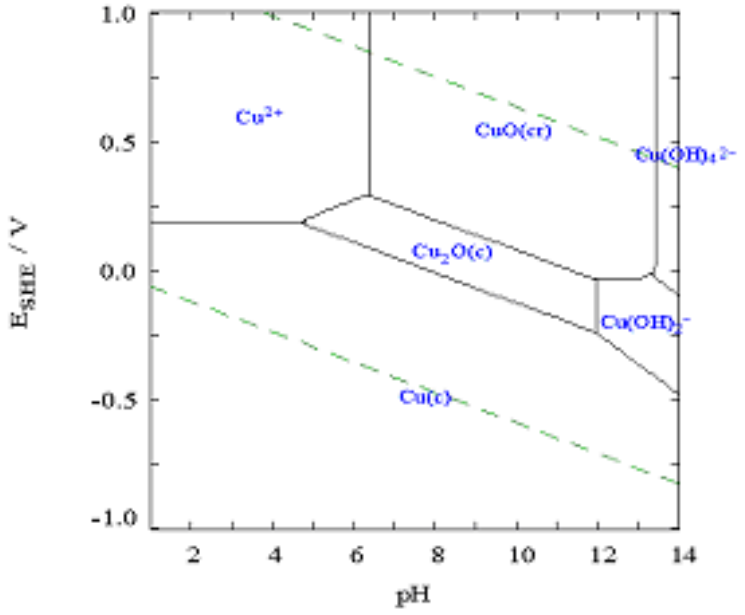

Figure 5.5 Pourbaix diagram for copper.

Thus cuprous oxide or any other copper mineral will be converted back to elemental copper by reacting with aluminum according to the following reaction.

$$2A1 + 3Cu_20 \rightarrow A1_2O_3 + 6Cu$$

Free energy of the above reaction is -92kcal/mol [8]. Copper is thus deposited on the surface and forms a galvanic cell with the adjacent aluminum. These sites are again favorable for formation of new pits and the entire material will be eventually consumed. Figure 5.6 shows a pictorial description of the pit growth process. The presence of copper deposits is evident from the micrographs in Figure 5.7 and EDS analysis in Figure 5.8. The bottom of the pit acts as anode and dissolution of aluminum gives Al^{3+} cations. The anodic reaction leaves behind electrons which are consumed at the copper sites on the surface for production of hydroxyl ions OH^-, a typical cathodic reaction in aerated water. Aluminum can get corroded in the pit in three ways. Due to migration of chloride ions in to the pit, formation of aluminum chloride $AlCl_3$ is possible. Formation of aluminum hydroxide $Al(OH)_3$ due to hydrolysis of water inside the pit which decreases the pH further is also possible. Dissolution of aluminum in the solution because of low pH is another possibility, which will be accompanied by hydrogen evolution [4].

$$Al_2O_3 + 6H^+ + 6Cl^- \rightarrow Al_2Cl_3 + 3H_2O$$

$$A1^{3+} + 3H_2O \rightarrow Al(OH)_3 + 3H^+$$

$$2A1 + 6H^+ \rightarrow 3H_2 + 2A1^{3+}$$

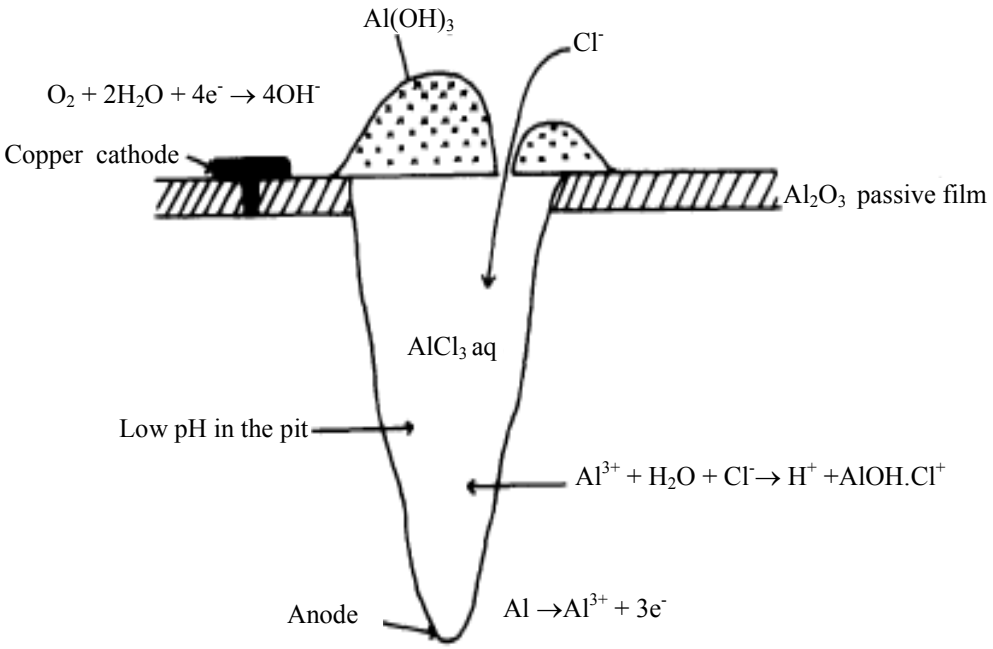

Figure 5.6 Process of pit growth in aluminum alloy 2024 in presence of chloride ions [4].

Although one might be tempted to think that higher the chloride content, the faster material is consumed. However, the potentiodynamic plots in Figure 4.18 show that even by increasing the concentration of chloride ions from 0.6M to 3M the critical pitting potential does not show much variation. Four samples tested in 0.6M, 1M, 2M and 3M sodium chloride solutions showed approximately the same pitting potential. This indicates that the chloride ion concentration has no effect on the rate at which pitting occurs. Figure 5.9 shows a plot of pitting potentials against the chloride ion concentration. Although, it would not be safe to assume that pitting occurs at all chloride ion concentrations and there is no threshold concentration at which pitting initiates.

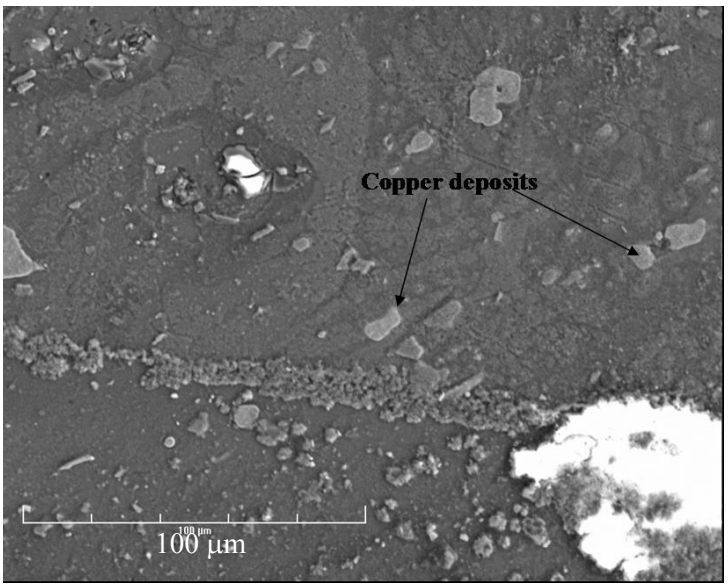

Figure 5.7 Copper deposits on the aluminum alloy surface.

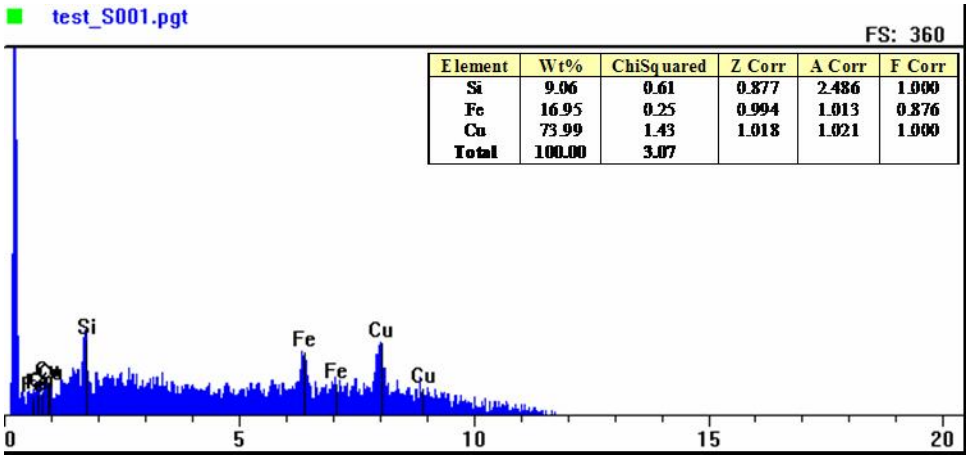

Figure 5.8 EDS for the areas rich in copper deposits.

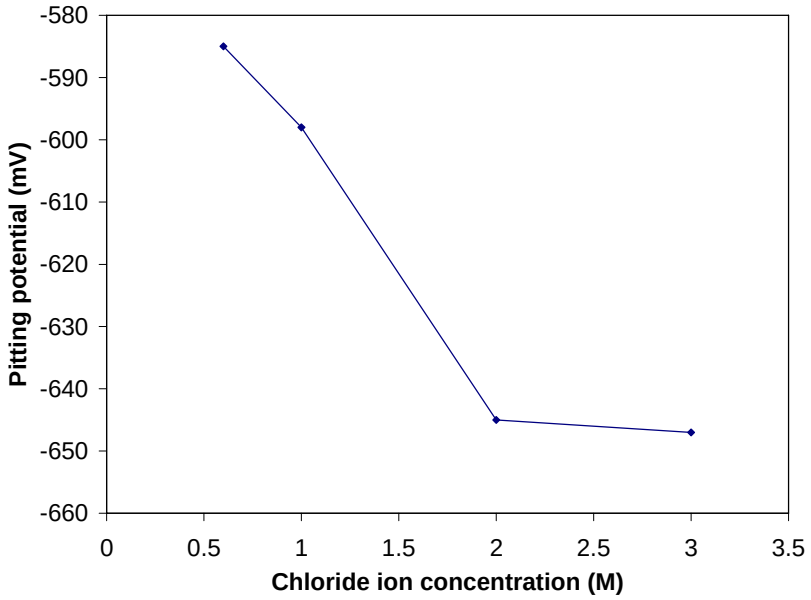

Figure 5.9 Pitting potentials measured against different sodium chloride concentrations.

Deterioration of materials in seawater is due to the cumulative effect of temperature, pH, dissolved oxygen, salinity and sea current. The aluminum alloys used in the early part of the 20th century contained copper as one of the major alloying elements. Copper helps to increase the mechanical properties of aluminum alloys [6]. However the corrosion resistance of such alloys is reduced. Copper is the cathode and sets up a galvanic cell with aluminum. Aluminum is the anode and is corroded preferentially [7]. The potentiodynamic plots in Figure 4.18 show that out of the two most abundant anions, chloride and sulphate anions, present in seawater, the chloride ions are the most aggressive towards initiation and growth of pits. The potentiodynamic plot for sodium sulphate electrolyte indicates no breakdown of the aluminum oxide layer and hence aluminum alloy shows no pitting in presence of sulphate ions alone.

Since the 1930s, other aluminum alloys have been introduced with a focus on improving the different mechanical and physical properties, so that they could be targeted for specific applications. Courtesy of ALCOA, Aluminum Company of America, Table 5.1 summarizes the properties and application of the modern day aluminum alloys used in the aerospace industry. Aluminum alloy 2024 was developed by ALCOA in the 1930s. Their high strength to weight ratio increased their demand in the aeronautical industry. Aluminum alloy 2024 is used as a material for fuselage and for skin even in the modern aeronautical industry. Aluminum alloy 2124 is an improved version of alloy 2024 having a higher fracture toughness and creep strength and creep strength. The 7XXX series was first introduced in 1940's. The 7XXX series has higher strength than the 2XXX series alloys, but the fracture toughness has a lower value compared to the 2XXX series. The 2XXX series shows better fatigue properties than the 7XXX series.

Table 5.1 Summary of aluminum alloys used in aerospace applications [Courtesy ALCOA][32].

Al alloy	Description	Application
2024	1. Introduced by Alcoa in 1931 as an alclad sheet. 2. Replaced 2017 Duralumin as prominent 2XXX alloy. 3. Major alloying element is copper upto 4.5%. 4. Good Fatigue and toughness charact	Fuselage structurals, wing tension members, shear webs and ribs and structural areas where stiffness, fatigue performance and good strength are required
2090	1. Aluminum lithium alloy. 2. Offers an 8 % density savings when compared with other aerospace alloys. 3. 10% higher elast	Aircraft floor bulkhead stiffeners to take advantage of the high strength and lower density to achieve a substantial weight reduction. Wing leading and trailing edges, fuselage bulkhead webs and internal framework parts
2124	1. Guaranteed fracture toughness. 2. Good strength retention and creep resistance at elevated temperatures up to 350° F. 3. Fracture toughness levels highe	Machined fuselage bulkheads and wing skins in high-performance military aircraft
2324	1. Higher strength and purity version of alloy 2024. 2. Improved strength and fracture toughness properties over alloy 2024.	Lower wing skin and center wing box components of new commercial transport aircraft
7050	1. Best combination of strength, stress corrosion cracking (SCC) resistance and toughness. 2. Alloy 7050 exhibits better toughness/corrosion resistance characteristics than alloy 7075.	Fuselage frames and bulkheads where section thicknesses are 2 to 6 inches.

Table 5.1 Continued

Al alloy	Description	Application
7055	1. Higher compressive and tensile strengths while maintaining other important properties such as fracture toughness and corrosion resistance as compared to alloy 7150	Upper wing structures, horizontal stabilizer, and keel beams. potential applications include seat and cargo tracks
7075	1. Al-Zn-Mg-Cu high strength alloy. 2. Good stress-corrosion cracking resistance.	Alclad skin sheet, thick structural plate components and general aluminum aerospace applications
7150	1. Highest strength aluminum plate. 2. Guaranteed levels of fracture toughness, higher than alloy 7075.	Upper wing skins on large commercial aircraft where high compressive yield strength is required
7475	1. A combination of high strength, superior fracture toughness and fatigue crack propagation. 2. 40% greater fracture toughness values than 7075	Can be considered for fuselage skins, wing skins, wing spars and fuselage bulkheads

6. PRE-RECOVERY SURVEY AND POST-RECOVERY CONSERVATION PLAN FOR SUBMERGED AIRCRAFT

The primary missions of archaeologists are to study, collect, preserve and interpret objects of historical significance. After recovery from the burial site, all artifacts start to deteriorate. Some may deteriorate very slowly and some faster than others, due to a variety of reasons. Proper preservation methods need to be devised in order for the future generations to relish viewing these valuable objects belonging to their rich history and culture. Whenever a wreckage site is found, one may miss out on valuable information in a haste to recover it. Therefore, it is essential to divide the recovery plan into pre-recovery and post-recovery segments. As shown in Figure 6.1 pre-recovery steps will mostly deal with visual assessment of the artifact to check for structural stability and the extent of damage that has occurred due to deterioration over number of years. It also deals with appropriate measurements of the wreckage site which help in understanding of the physical, chemical and environmental information associated with the wreck site. This information might prove of great importance in studying the deterioration of the artifacts and in devising a preservation method. Post-recovery segment will deal with ways to try to restore the artifacts to their original manifestation. It involves handling, cleaning, deterioration control and storage of artifacts. The following guidelines are proposed for preservation of historic artifacts.

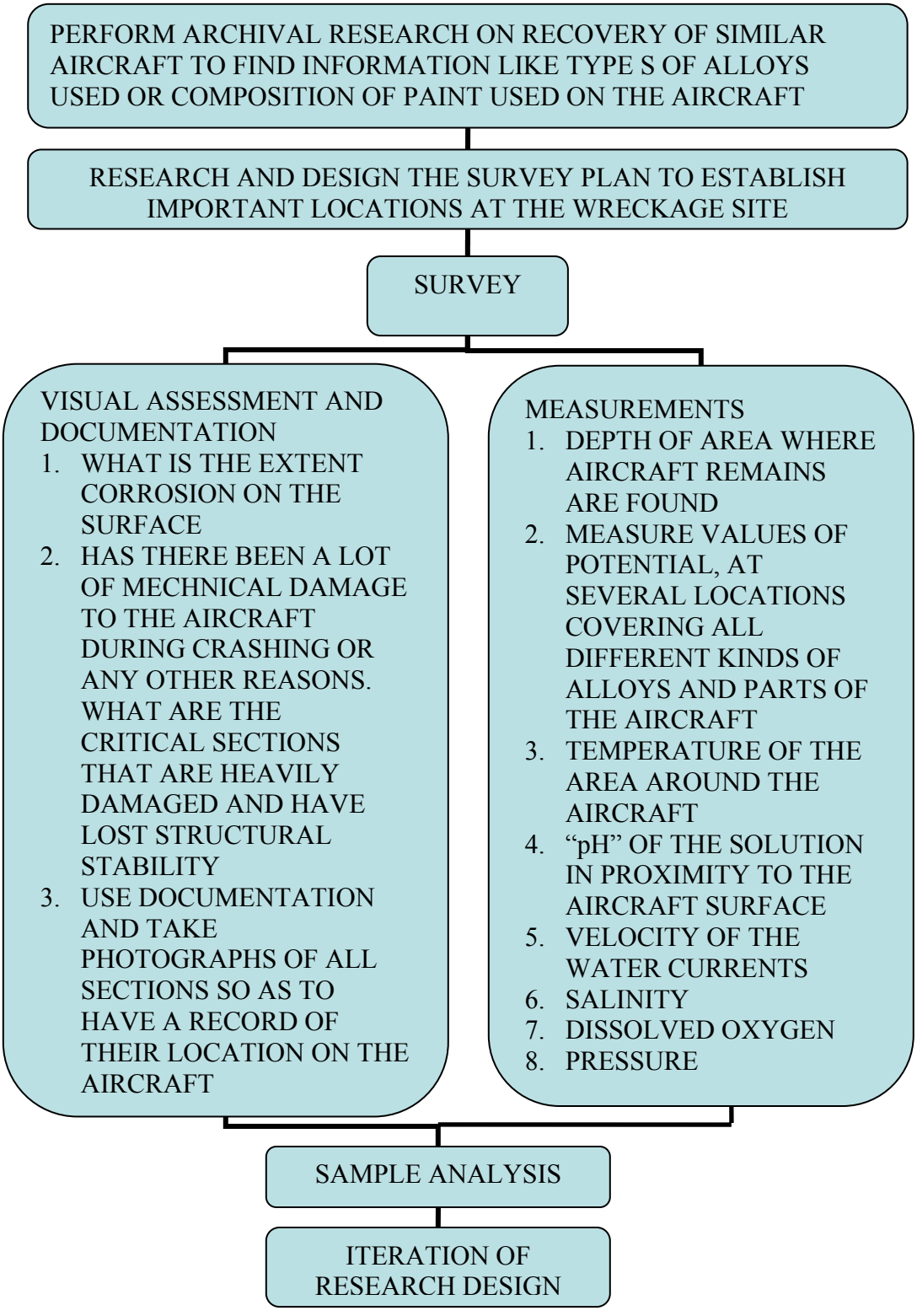

Figure 6.1 Pre-recovery research, assessment and survey plan.

6.1 Pre-recovery plan

When a submerged aircraft is found, the first step is to research some of the similar submerged aircraft case studies and gain knowledge of the procedure that was followed to recover the aircraft. It also helps to gain knowledge about the metal alloys that were used to manufacture the aircraft. Other information like the type of paint or coatings that were applied to the aircraft may prove useful in deciding the samples that need to be collected from the actual wreckage. The next step consists of planning the actual survey and establishing the important locations at the wreckage site, so that these areas could be a focus of sample collection, documentation and photography. Visual assessments of the wreckage and measurements that need to be taken at the wreckage site need to be planned before the actual dive. Aircraft using aluminum metal as a building material undergo a significant amount of pitting on the surface [4]. A visual assessment of the surface corrosion will give a brief idea about the damage occurred. A survey of the corroded surface over a sample area gives an idea about extent of material lost due to corrosion and helps in assessment of load the material can carry if a decision is made to lift the aircraft from seawater. Apart from the surface assessment one should also survey the aircraft for structurally weak sections. These sections may be a cause of failure during recovery although the overall appearance may suggest a safe lifting procedure. This damage might be caused during the aircraft crash or due to some other unforeseen reasons. The wreckage site should be photographed thoroughly and detailed photographs of critical sections should be taken. These photographs can be used as fingerprints in tracing back the conditions that existed around the object. Site monitoring

and surveillance is performed for various reasons Pre-recovery surveys deliver a baseline understanding of the physical, chemical and environmental information associated with the wreck site. The type of data gathered is a mixture of qualitative and quantitative data, for example, an unwritten portrayal of the sea conditions as compared to measurement of the water's pH. Other measurements like depth, salinity, temperature, pressure, dissolved oxygen and velocity of currents help in simulating in situ conditions needed while studying the behavior of the alloys in seawater. Measurement of corrosion potentials or E_{corr} values will help to make an assessment about the further deterioration of the aircraft. After the collection of samples, they will be sent to the lab for analysis and further iterations to the research design can be made based on the results obtained.

6.2 Post-recovery plan

Post-recovery plan consists of four steps. One should not handle artifacts using bare hands. The oils, acids and salts in human skin will damage most types of materials over time. Use of clean and dry hands is recommended while handling small artifacts. Wearing gloves may get rid of this problem. All artifacts should be treated as if they are extremely delicate, even if they do not appear so. It is also important to know the history of the artifact so that you’re aware of any previous damage, repairs, loose parts or weak spots. Avoid picking up objects by handles, straps or other protruding components. Ideally, artifacts should be handled one at a time. Before moving any artifact, make sure you have a clear place to set it. Finding a center of gravity of irregular objects is a difficult task. But whenever an object needs to be lifted make sure that the load applied

is as close to the center of gravity as possible in order to avoid toppling or tumbling of objects. One needs to decide if use of hooks should be used to lift the aircraft from seawater or whether using a net would serve the purpose. This decision is based on case to case basis, depending upon factors like the structural strength and location of weak section on the aircraft. Calculation of the drag forces that the aircraft may experience is important from the point of view of maintaining the structural stability of the aircraft. Also it is important to decide whether the load needed to lift the aircraft should be applied symmetrically in case some of the sections are weak. Aircrafts which have been under water for several years may develop a layer of calcareous deposit on the surface. This layer can sometimes be very tough to remove. Using a metal bristle brush can sometimes help to chip off these deposits. If the use of brush does not help to clean up all the deposits then one may use a pneumatic scribe to chip off the deposits. Ultrasonic cleaning is also used to achieve the same purpose. Use of tap water to clean any biofouling or slime is recommended. Washing and drying with distilled water may help wash away most of the chloride ions, which as already discussed are the major contributors to aluminum corrosion. Another way of arresting pitting and stop further deterioration of aluminum alloys is to remove any traces of electrolytes in the pits itself. In the absence of electrolytes corrosion is not possible. Using special vacuum suction cleaners may help to pull out water in the pits. Heating the artifacts in a controlled chamber can also help expedite the process of water removal from the pits by evaporating it. The stepwise procedure is as shown in Figure 6.2.

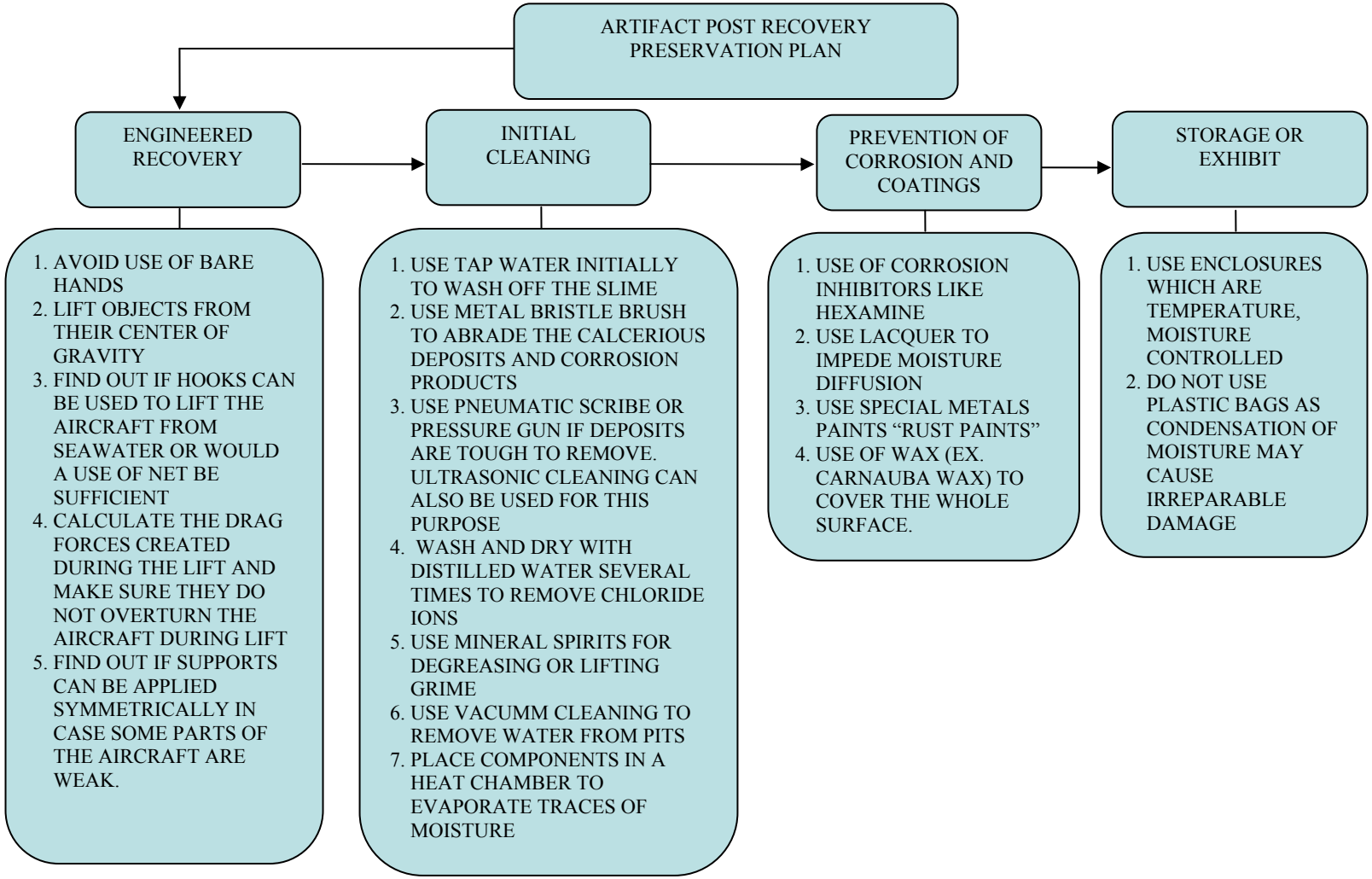

Figure 6.2 Post-recovery plan for submerged aircraft.

Next step is to prevent corrosion by using coatings or inhibitors. After complete drying, the artifact should be thoroughly degreased with reagent grade ethanol, acetone or methyl ethyl ketone. Corrosion inhibitors like hexamine, phenylenediamine, dimethylethanolamine, sodium nitrite, cinnamaldehyde, condensation products of aldehydes and amines (imines), chromates, nitrites, phosphates, hydrazine, ascorbic acid, can be used to slow down damage due to corrosion [33]. Application of lacquer may isolate the metal surface from the environmental moisture. Grease from handling will prevent lacquer from adhering to the surface. Cellulose nitrate or acrylic lacquers are preferable. Among the products commonly used are Agateen, commonly known as cellulose nitrate, and Acryloid B-72. The lacquer may be applied either by brushing or spraying. The application should always consist of two layers, to insure complete coating. Covering the metal surface with paints may help to arrest corrosion. But applying paint may sometime not be a feasible solution as it changes the original appearance of the structure. If there are small punctures in the applied paint then a situation may arise in which you have a large cathode, in this case the area which still has a layer of paint and a small anode, the areas which are devoid of paint. Pitting corrosion in this case can be at a faster rate than compared to a surface which is not painted. Using wax, for example carnauba wax, is also a commonly used practice in order to isolate the metal surface from exposure to external environment. The only problem with wax covering is that it should not be exposed to fluctuating temperature conditions. Cracks may develop in the wax surface due to indifferent expansion and contraction due to temperature changes and again one might just accelerate the pitting

corrosion process instead of arresting it. Corrosion inhibitors are chemical compounds added to the corrosive medium to reduce the rate of its attack on the metal or alloy. The chemicals which can act as corrosion inhibitors may be inorganic or organic. The inorganic compounds such as chromates inhibit the corrosion process via formation of passive oxide film on the metal surface and thus prevent the corrosive medium to attack the bar metal. On the other hand, the organic compounds settle on the metal surface forming a barrier between the metal and the corrosive environment. Some structural features of the organic compounds help them to do so. These include the presence of oxygen, nitrogen or sulfur atoms as well as presence of double bonds [34].

Providing a properly controlled and stable environment is critical to the long-term preservation of the museum's artifacts. The ideal levels vary, however, depending on the type of artifact in question. A constant temperature between 68 to 72 degrees and humidity levels of approximately 42-46 % are favorable for artifact stability [15]. More important than achieving those particular numbers, however, is maintaining a steady environment. Variation is what causes the most damage. The temperature and relative humidity levels inside a building with no heating, ventilating and air condition system fluctuate widely with the heating of the day and then cooling of night. Daily variations are more dangerous than seasonal ones. The ideal conditions should be maintained at all times.

7. CONCLUSION AND FUTURE WORK

The composition of the aluminum alloys used to manufacture '*Carnauba*' S-38 aircraft confirm with aluminum alloy 2024 with copper as the primary alloying element. Dispersion of intermetallics of copper, aluminum and magnesium is found to exist in the aluminum matrix. These intermetallics are inconsistent in size and are randomly distributed. The inhomogeneous distribution of copper intermetallics and the difference in the potentials between the aluminum matrix and the intermetallics sets up a local galvanic cell. The aluminum matrix acts as anode and is corroded in presence of an electrolyte like seawater. The galvanic cells act as sites for localized corrosion and are potential sites for pitting. The chloride ions are adsorbed through the aluminum oxide film and react with the surface aluminum to cause metal chlorides. This causes a decrease in the pH in a small local region and increases the chances for pitting corrosion. The copper and aluminum in the pit area are oxidized, but as aluminum oxides are more stable than cuprous oxide for conditions existing in seawater, the cuprous oxide is converted to copper and deposits itself on the surface of the alloy. The potential difference between copper and aluminum is even more than that between copper intermetallics and aluminum. This gives rise to additional sites which are favorable for localized corrosion and increases the chances of pitting. In order to retard the pitting one has to either extract the chloride ions from the pits or increase the pH to make the conditions inside the pit tending towards neutral. This study has not only importance from point of view of historical artifacts but also from point of view of the modern day

aeronautical industry, as aluminum alloy 2024 is still used as a material for fuselage and skin construction.

When an aircraft needs to be recovered from seawater, an engineered recovery involving the type of loading, location of loading, proper documentation and photography of the critical sections need to be planned. Prior archival research on similar recoveries helps not to commit the same mistakes and also to find out information regarding the fabrication of the aircraft. Post-recovery, careful steps towards cleaning and proper handling of the aircraft need to be taken as chances of structural damage are maximum during these two steps. Corrosion inhibitors in conjunction with coatings should be used to mitigate the damage due to corrosion and preserve the aircraft for as long as possible.

7.1 Future work

Little or no information is available regarding effect of inorganic corrosion inhibitors like nonhalide anions such as sulfates or nitrites and organic inhibitors such as Bacillus biofilms secreting polyaspartate or γ-polyglutamate [35] in mitigating corrosion of aluminum alloy 2024. Also one needs to take into consideration the microbiologically influenced corrosion of aluminum alloy 2024 and its aid in the pitting corrosion of the alloy. Parts made up of material other than aluminum alloy 2024 need to be treated differently in order to preserve them and hence have a tremendous scope of further study.

REFERENCES

1. Child; R., and Townsend, J., 'Modern metals in museums', *Studies in Conservation* **35**(3) (1990) 167-167.
2. Lacoudre, N., 'Electricité et archeologie', *Fana de l'Aviation* **184 (**1985**)** 11-12.
3. Bousquet, G., 'Les Dornier oubliés du lac de biscarrosse', *Fana de l'Aviation* **144 (**1980**)** 43-47.
4. MacLeod, I.D., 'Stabilization of corroded aluminium', *Studies in Conservation* **28**(1) (1983) 1-7.
5. Adams, C.D., *Treatment of the BMW 801D-2 Radial Aero Engine Rescued from the Loiret River*, Australian War Memorial Publication, Canberra (1992).
6. Wyss, R.K., 'Microstructure-property relationship in a 2XXX aluminum alloy with Mg addition', *Metallurgical and Materials Transactions.* **19A**(10) (1988) 2523-2530.
7. Szklarska-Smialowska, Z., 'Pitting corrosion of aluminum', *Corrosion Science* **41** (1999) 1743-1767.
8. Obispo, H.M., Murr, L.E., Arrowood, R.M., and Trillo, E.A., 'Copper deposition during the corrosion of aluminum alloy 2024 in sodium chloride solutions', *Journal of Materials Science* **35** (2000) 3479–3495.
9. LaQue, F.L., *Marine Corrosion*, John Wiley and Sons Inc., New York (1975).
10. Grobe, H., 'Elemental composition of seawater', http://en.wikipedia.org/wiki/Image:Sea_salt-e_hg.svg (accessed May 2, 2008).

11. Jones, D.A., *Principles and Prevention of Corrosion*, 2nd edn, Macmillan Publishing Company, New York (1992).
12. Venkatesan, R., *Studies on Corrosion of Some Structural Materials in Deep Sea Environment*, Ph.D. Thesis, Indian Institute of Science, Bangalore (2000).
13. Lewis, E.L., 'The practical salinity scale 1978 and its antecedents', *Journal of Oceanographic Engineering* **5**(1) (1980) 3-8.
14. Pearson, P.N., and Palmer, M.R., 'Middle eocene seawater pH and atmospheric carbon dioxide concentrations', *Science* **284**(5421) (1999) 1824–1826.
15. Heidersbach, R., 'Marine corrosion - specific industries and environments, Corrosion', *ASM Metals Handbook* **13** (1986) 893-926.
16. Corrosion Technology Laboratory Kennedy Space Center , 'Uniform corrosion illustration', http://corrosion.ksc.nasa.gov/unifcor.htm (accessed May 2, 2008).
17. Galvanizeit, 'Galvanic Corrosion Cell', http://www.galvanizeit.org/showContent, 272,316.cfm (accessed May 2, 2008).
18. Corrosion Technology Laboratory Kennedy Space Center , 'Galvanic corrosion illustration', http://corrosion.ksc.nasa.gov/galcorr.htm (accessed May 2, 2008).
19. Corrosion Technology Laboratory Kennedy Space Center , 'Crevice corrosion illustration', http://corrosion.ksc.nasa.gov/crevcor.htm (accessed May 2, 2008).
20. Lula, R.A., Davis, J.A., and Steigerwald, R.F. (ed.), 'Intergranular corrosion of stainless alloys', *ASTM STP* **656** (1978) 233-247.
21. Whitcraft, P.K., 'Corrosion of stainless steel', in *Corrosion Engineering Handbook*, ed. P. Schweitzer, 11th edn, Marcel Dekker, New York (1996) 53-77.

22. Laboratoire de Physicochimie Industrielle, 'Model of pitting corrosion, http://www.cdcorrosion.com/mode_corrosion/corrosion_crevice.htm (accessed May 2, 2008).
23. Corrosion Technology Laboratory Kennedy Space Center , 'Pitting corrosion illustration', http://corrosion.ksc.nasa.gov/pittcor.htm (accessed May 2, 2008).
24. Sikorsky Aviation Corporation, *Sikorsky Amphibian S-38,* College Point, New York (1929).
25. Buehler, 'Recommendations for etching', http://www.buehler.com/technical information/Buehler%20Book/etching.pdf (accessed May 7, 2007)
26. ASM Handbooks online, 'Properties of wrought aluminum and aluminum alloys', *ASM International* **2** (2007) Table 22.
27. Ying Li, Trillo, E.A., and Murr, L.E., 'Friction-stir welding of aluminum alloy 2024 to silver', *Journal of Materials Science Letters* **19**(12) (2000) 1047-1051.
28. Di Schino, A., and Kenny, J.M., 'Effect of grain size on the corrosion resistance of a high nitrogen-low nickel austenitic stainless steel', *Journal of Materials Science Letters* **21**(24) (2002) 1969-1971.
29. Kaufman, J.G., and Rooy, E.L., *Aluminum Alloy Castings: Properties, Processes, and Applications*, ASM International, Materials Park, Ohio (2004)
30. Liao, M.C., and Wei, R.P., 'Galvanic coupling of model alloys to aluminum - a foundation for understanding particle-induced pitting in aluminum alloys', *Electrochimica. Acta* **45** (1999) 881-888.

31. Muster, T.H., Hughes, A.E., Harvey, T.G., Nikpour, T., and Hardin, S.G., 'The etching of aluminium alloy 2024-T3 in a non-chromate Fe(III)-HF HNO_3 deoxidiser: an atomic force and scanning kelvin microscopy study', *Materials Forum* **28** (2004) 1243-1248.
32. Alcoa, 'Properties and applications of aluminum alloys', http://www.alcoa.com/aerospace/en/products/overview.asp (accessed February 9, 2008)
33. Fontana, M.G., *Corrosion Engineering*, 3rd edn, McGraw-Hill, New York (1986).
34. El-Etre, A.Y., 'Inhibition of aluminum corrosion using opuntia extract', *Corrosion Science* **45** (2003) 2485-2495.
35. Örnek, D., Jayaraman, A., Syrett, B.C., Hsu, C.H., Mansfeld, F.B., and Wood, T.K., 'Pitting corrosion inhibition of aluminum 2024 by bacillus biofilms secreting Polyaspartate or γ-Polyglutamate', *Applied Microbiology and Biotechnology* **58** (2002) 651-657.

VITA

Name: Kedar Gujarathi

Address: Texas A&M University, Department of Mechanical Engineering, 3123 TAMU, College Station, TX 77840, USA

Email Address: guja11@tamu.edu

Education: B.En, Mechanical Engineering, University of Pune, India, 2005

M.S, Mechanical Engineering, Texas A&M University, College Station, Texas, 2008